

THE PENNSYLVANIA STATE UNIVERSITY
SCHREYER HONORS COLLEGE

DEPARTMENT OF BIOCHEMISTRY & MOLECULAR BIOLOGY

The Toll of SARM1/TIR-1—A Novel NAD⁺-Consuming Enzyme

IAN ARGENTO
SPRING 2024

A thesis
submitted in partial fulfillment of the requirements
for a baccalaureate degree
in Biochemistry & Molecular Biology
with honors in Biochemistry & Molecular Biology

Reviewed and approved* by the following:

Dr. Melanie McReynolds
Assistant Professor of Biochemistry and Molecular Biology
Thesis Supervisor

Dr. Lorraine Santy
Associate Professor of Biochemistry & Molecular Biology
Honors Adviser

* Electronic approvals are on file in the Schreyer Honors College.

ABSTRACT

The discovery that nicotinamide adenine dinucleotide (NAD⁺) declines with age launched scrutiny into the web of metabolic pathways that produce and consume the essential cofactor. Recently, the scrutiny befalls SARM1—a novel NAD⁺-consuming enzyme with implications in neuronal cell death. While researchers examine the potential boon to NAD⁺ and neural health offered by SARM1 knockdown therapeutics, I seek to understand how SARM1 deletion affects the organism as a whole: what uncharacterized phenotypes associate with SARM1 deletion, and how do they relate to altered NAD⁺ metabolism?

I begin my research into the SARM1 homologue TIR-1 found in *C. elegans*, where I examine longevity, brood-sizes, and NAD⁺ metabolism to characterize the health (and illness) of TIR-1 mutants. My data suggests that the evolutionarily conserved NAD⁺-consumer maintains health, promoting a longer lifespan and increased reproductive vitality without significantly depleting NAD⁺. I explore metabolomics data to understand a potential role for TIR-1 not in NAD⁺ consumption, but in mediating the uptake of NAD⁺ precursors. My research contributes to the ongoing investigation of how to protect against NAD⁺ imbalance and offers insight on how *C. elegans* TIR-1 mutants model therapeutics which target SARM1.

TABLE OF CONTENTS

LIST OF FIGURES	iii
ACKNOWLEDGEMENTS	v
Chapter 1 Introduction	1
Age-Related NAD ⁺ Decline	1
A Not-So-Novel NAD ⁺ Consumer	4
TIR Domains.....	4
Choosing <i>C. elegans</i>	5
NAD ⁺ Pathways in Humans Versus the Worm	6
SARM1/TIR-1 NAD ⁺ Consumption.....	9
A Brief SARM1 History	9
Mechanism of SARM1 activation	11
TIR-1 Stress Mediation.....	12
Conclusion	14
Chapter 2 Materials and Methods	15
<i>C. elegans</i> Strains and Maintenance	15
Brood Size Assays and Lifespan Assays	15
Multigenerational Live-Food Metabolomics	16
Data Analysis.....	16
Chapter 3 Results	17
The Effect of TIR-1 on Longevity	17
The Effect of TIR-1 on Reproductive Health	22
The Effect of TIR-1 on NAD ⁺ Metabolism	24
Role of TIR-1 in the <i>De Novo</i> Pathway	24
Role of TIR-1 in Redox States.....	31
Role of TIR-1 in NR Homeostasis.....	32
Role of TIR-1 in NAD ⁺ Consumption	34
Role of TIR-1 in the Salvage Pathway.....	37
Role of TIR-1 in Global Metabolism.....	38
Chapter 4 Discussion	41
Necessity of Standardizing Longevity Assay Graphs.....	41
Reproductive Assays as Measurements of Stress-Tolerance.....	43
Statistical Significance of Metabolomic Data.....	45
TIR-1 Shunts Tryptophan into the <i>De Novo</i> Pathway	46
TIR-1 Shunts Kynurenine out of the <i>De Novo</i> Pathway.....	46
Immune Pathways and <i>De Novo</i> Regulation	47

Oxidation in TIR-1 Mutants.....	48
Altered NR Pathway in TIR-1 Mutants	48
A Lackluster NAD ⁺ Consumer.....	49
Overactive Salvage Pathway.....	50
Appendix.....	51
List of Abbreviations in Order of Appearance	51
Funding Acknowledgment.....	52
BIBLIOGRAPHY.....	53

LIST OF FIGURES

Figure 1: Hallmarks of Aging and NAD ⁺ Decline.....	2
Figure 2: The Invariant <i>C. elegans</i> Life Cycle	6
Figure 3: The Kynurenine/ <i>De Novo</i> Pathway.....	7
Figure 4: NAD ⁺ Metabolism.....	8
Figure 5: The SARM1 Bear Trap	12
Figure 6: TIR-1 and SARM1 Sequence Similarity.....	13
Figure 7: Kaplan-Meir Survival Curves of TIR-1 Mutants Compared to N2	18
Figure 8: Gaussian Distributions of Strain Longevity	20
Figure 9: Average Longevity of TIR-1 Mutant Strains Compared to N2	21
Figure 10: Brood-Size of TIR-1 Mutant Strains Compared to N2	23
Figure 11: Percent of Worms that Internally Hatch.....	23
Figure 12: Comparison of Kynurenine and Tryptophan Levels Across TIR-1 Mutant Strains	25
Figure 13: Comparison of Indole Pathway Metabolites Across TIR-1 Mutant Strains	27
Figure 14: Comparison of Kynurenine and 3-Hydroxyanthranilic Acid Levels Across TIR-1 Mutant Strains.....	28
Figure 15: Correlation Between the Fold Change in Kynurenine and the Fold Change in 3- Hydroxyanthranilic Acid	30
Figure 16: NaMN Total Ion Count in TIR-1 Mutant Strains.....	31
Figure 17: Comparison of Redox Couples Between TIR-1 Mutant Strains.....	32
Figure 18: NAD ⁺ Total Ion Count in TIR-1 Mutant Strains.....	33
Figure 19: Metabolites of the NR Pathway Normalized to NR.....	34
Figure 20: Comparison of NAM and NAD ⁺ Levels Across TIR-1 Mutant Strains	35
Figure 21: Comparison of ADPR Breakdown Metabolites Across TIR-1 Mutant Strains	37
Figure 22: NAM to NA Turnover in TIR-1 Mutant Strains	38
Figure 23: Global Metabolite Heatmaps.....	40

ACKNOWLEDGEMENTS

I'd like to thank Dr. McReynolds, my PI and thesis advisor, for her trust. She welcomed me to her team as her first undergraduate researcher. It has been a privilege to watch the lab grow and to work with the excellent team she cultivates. I thank Kareem for his patience as he taught me how to perform lab work; I thank JJ for his friendship in our first summer at the lab and for helping me collect brood-size and longevity data; I thank Alex for the passion she brings, our many late night talks over bench-work, and for the time she helped me fish out samples I dropped in a vat of liquid nitrogen; I thank Kelly for her encouragement as I wrote this thesis. I would not be here without all of your support.

Chapter 1

Introduction

Age-Related NAD⁺ Decline

The modern lifespan exists as one of humanity's most astonishing feats. Over the last century (a timeframe that only modern humans could expect to experience) the average lifespan of a newborn doubled¹. Life expectancy did not just rise for children—so did the expected lifespan for all age groups². Public health advancements in hygiene, vaccines, antibiotics, diagnostic testing, and medical interventions confront aging populations with two central questions: what is the limit of the human lifespan, and as old age becomes older, how do populations retain their health, not just their years?

The essential cofactor nicotinamide adenine dinucleotide (NAD⁺) sits at the crux of both questions. NAD⁺ mediates over 500 reactions in the human metabolism³. If electrons are the currency of a chemical reaction, NAD⁺ functions as a middleman, interconverting between NAD⁺ and NADH to carry electrons from seller to buyer. As the key regulator of cellular bioenergetics, NAD⁺ impacts nearly all biological processes: deficiencies result in neurological, cardiovascular, metabolic, and degenerative disease, and scientists recognize NAD⁺ decline as a hallmark of aging⁴. Understanding why NAD⁺ declines with age and how restoring balance may protect against age-related disease presents an attractive avenue for research.

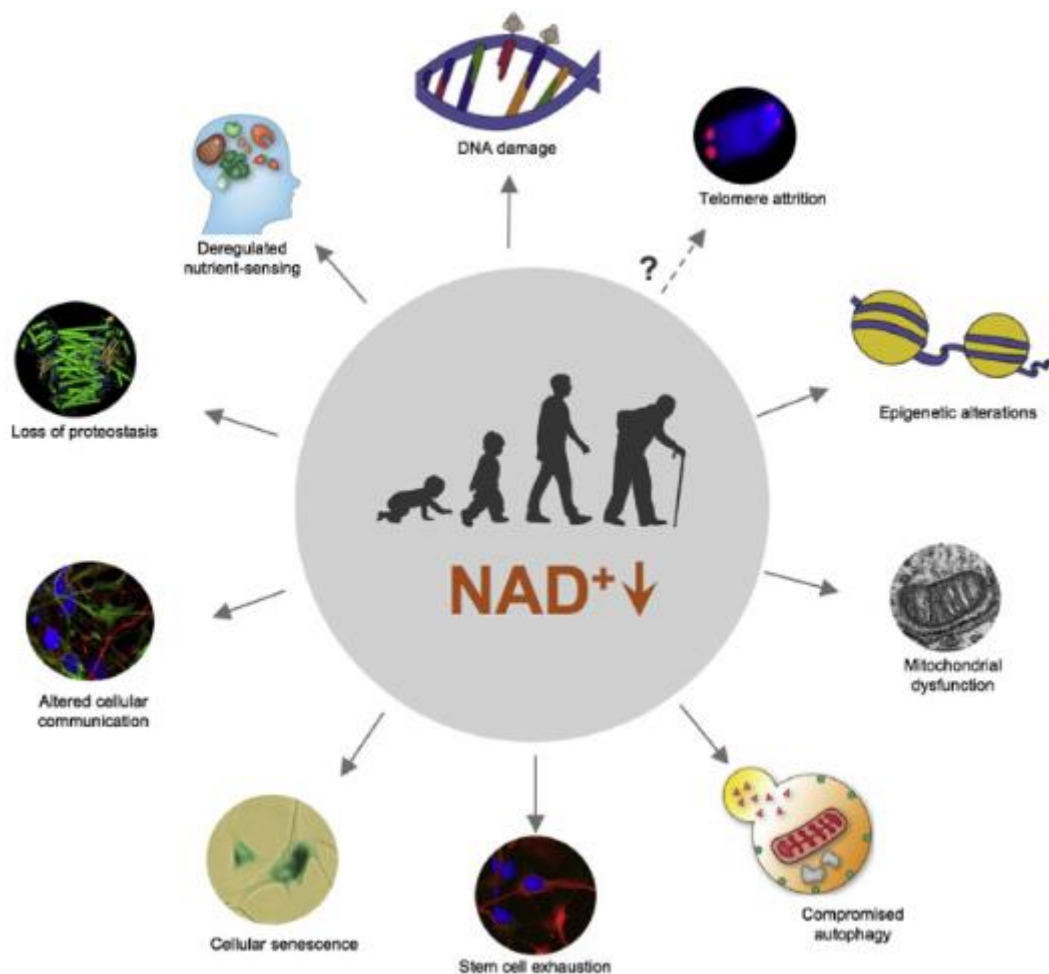


Figure 1: Hallmarks of Aging and NAD^+ Decline

Figure from Aman *et al.* 2018⁵

Isotope tracing experiments indicate that an age-related increase in NAD^+ -consumer activity drives NAD^+ decline⁶. The literature centers on three traditional classes of NAD -consumers: sirtuins, poly ADP-ribosyl polymerases (PARPs), and cyclic ADP-ribose synthases (CD38/CD157). While sirtuin activity seems to promote longevity⁷, sirtuins compete⁶ against the

anti-longevity PARPs⁸ and CD38⁹ for a limited pool of NAD⁺. Worse, sirtuin levels decline with age¹⁰ while the activity of PARPs and CD38 increase, driven by their respective roles in repairing DNA damage and mediating inflammation⁶. The repair-driven activity of NAD⁺ consumers support the finding that consumers upregulate over the aging trajectory.

The toll of a fourth NAD⁺-consumer—SARM1—remains relatively unexplored. Under conditions of axonal stress, SARM1 activates to deplete local NAD⁺ stores and kill the neuron¹¹. Researchers study SARM1 as a promising target for neuroprotective therapeutics, finding that SARM1 deletion protects against traumatic brain injury¹², increases Schwann-cell resistance to chemotherapy¹³, alleviates degeneration in diabetic peripheral neuropathy¹⁴, and reduces amyloid beta plaques in mouse models of Alzheimer's disease¹⁵.

However, perhaps because the NAD⁺-consuming activity of SARM1 was identified as recently as 2017¹⁶, research on SARM1's impact beyond the axon remains negligible. Despite extensive research into PARPs, CD38, and sirtuins, no research exists on SARM1's impact on global metabolism. Little exists on SARM1's toll on overall health. In my thesis, I aim to uncover the global effects of TIR-1, the *Caenorhabditis elegans* homologue of SARM1. By examining the consumer's toll on longevity, reproductive health, and NAD⁺ metabolism, my research serves the world's aging population by informing therapeutics while bridging the connections between stress, metabolism, and health.

A Not-So-Novel NAD⁺ Consumer

Although researchers only recently discovered SARM1's ability to cleave NAD⁺ and kill neurons, SARM1 is evolutionarily ancient, conserved across all domains of life. Functional SARM exists in mice, flies, nematodes, even the "living fossil" horseshoe crab^{17,18}; SARM's "TIR" domain which mediates NAD⁺-cleavage extends to archaea, bacteria and plants¹⁹. Understanding that SARM1 and its TIR domain exist as irreplaceable facets of evolution contextualizes the need for further study, especially as current research promotes the health benefits of SARM1 inhibition.

TIR Domains

TIR domains, like the one in SARM1, connect cytosolic "adaptor proteins" with proteins that pass through the cell membrane and detect extracellular pathogens²⁰. Transmembrane proteins peer through a cell's membrane to keep tabs on the environment, like the periscope on a submarine. When the periscope spots danger, an alarm alerts the captain to mediate a response. TIR domains function like the alarm, activating under stress and danger to call the intracellular adaptor protein to action.

Five TIR-containing adaptor proteins direct the signaling cascades that lead to the innate immune system response in human cells. Four propagate signaling cascades while the fifth, SARM1, inhibits signaling cascades²¹. SARM1 is the only adaptor protein whose TIR domain has been

shown to cleave NAD⁺²². SARM1 is also the only TIR-containing adaptor protein with a clear orthologue in *C. elegans*²¹.

Despite SARM1's down regulating activity in the immune system, the *C. elegans* orthologue TIR-1 upregulates the innate immune system by propagating a p38 MAPK signaling pathway²³. In compensation, *C. elegans* lack CD38²⁴, an NAD⁺-consuming enzyme which confers pathogen resistance in animal models²⁵. An area of further research could explore if SARM1 evolved to develop anti-immune activity only after pairing with pro-immune CD38. Research that demonstrates how both TIR-1/SARM1 and CD38 both regulate Ca²⁺ signaling through the same products of NAD-cleavage²⁶ supports the possibility that TIR-1 may function dually as both SARM1 and CD38 in the nematode.

Choosing *C. elegans*

Studying TIR-1 in *C. elegans* rather than SARM in humans or other mammals offers advantages. Few eukaryotes have a longer tradition in aging and nervous system research than *C. elegans*^{27,28}. The worms are transparent, meaning that researchers can visualize individual neurons, their connections, synapse formation, and neural degeneration real-time in the living organism²⁸. *C. elegans* also reproduce rapidly, develop invariantly (making it easy to spot phenotypic differences), live less than a month (making longevity assays time-efficient), and best of all for the beginner researcher, they are simple to store and handle²⁷.

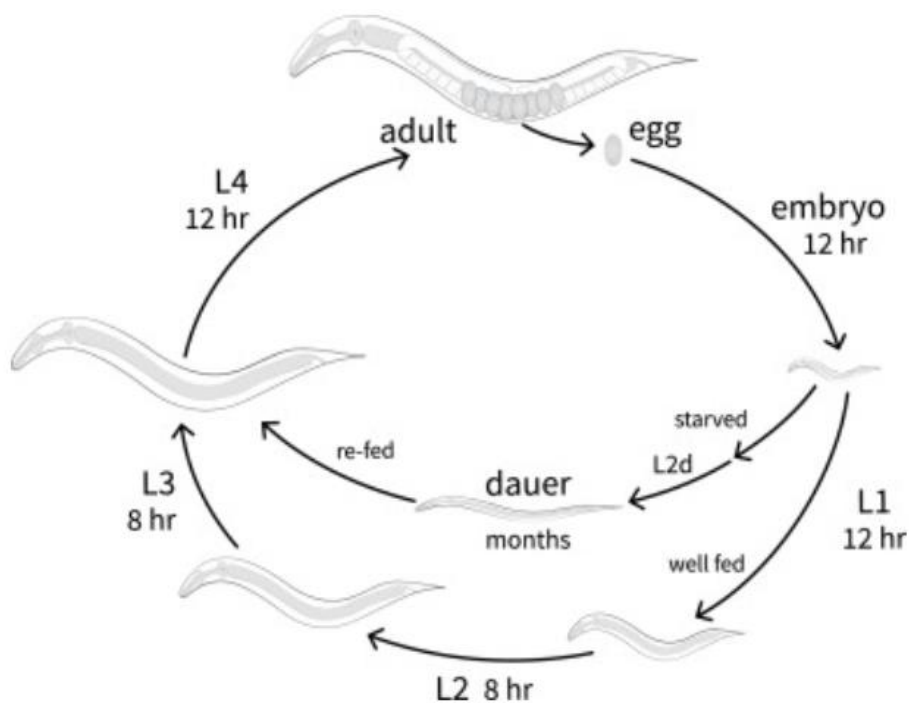


Figure 2: The Invariant *C. elegans* Life Cycle

Figure from Kimble *et al.* 2022²⁹

NAD⁺ Pathways in Humans Versus the Worm

Importantly, nearly 40% of genes involved in human disease are phylogenetically identical to the worm²⁷—genes which affect health in *C. elegans* likely affect health in humans, too. Humans and worms share three conserved pathways that regulate NAD⁺ biosynthesis: the *de novo*, Pries-Handler and salvage pathways³⁰.

The *de novo* pathway describes NAD⁺ production from exogenous resources. Both worms and humans must consume the essential amino acid tryptophan in their diet because neither produces the molecule endogenously. In the *de novo* pathway, several enzyme-supported reactions convert

tryptophan into quinolinic acid. While humans and worms share homologues for the five enzymes that turn tryptophan into quinolinic acid, they do not share a homologue for the enzyme that converts quinolinic acid into NaMN, a molecule that feeds into the Pries-Handler pathway. Instead, worm metabolism relies on an evolutionarily unrelated enzyme that catalyzes the same reaction.

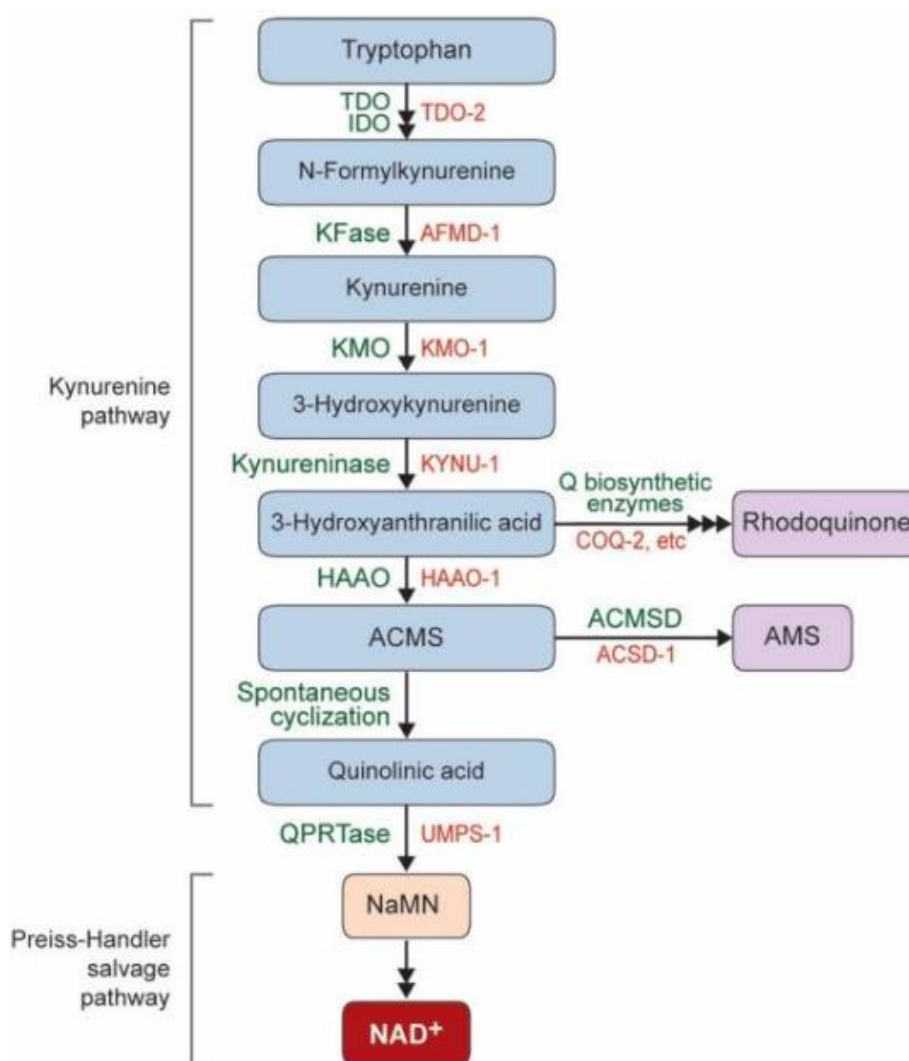


Figure 3: The Kynurenine/De Novo Pathway

The “kynurenine pathway” and “de novo pathway” are synonyms. Human enzymes are listed in green while *C. elegans* homologues are written in orange. Figure from Lee *et al.* 2020³⁰.

Exogenous and endogenous metabolites fuel the Pries-Handler pathway. Endogenous quinolinic acid converts into NaMN and so does nicotinic acid, which like tryptophan, can be found in the diet. In two conserved steps, NaMN converts into NAD^+ . Finally, NAD^+ consumers (like CD38, sirtuins, PARPs, and SARM1) cleave NAD^+ to form NAM, which recycles through the salvage pathway.

In the salvage pathway, humans convert NAM into NMN, a direct precursor to NAD^+ . Aside from NAD^+ consumers, NAM comes from nicotinamide riboside, the third and final NAD^+ precursor found exogenously in the diet. Worms lack the necessary enzyme to convert NAM directly into NMN. Instead, they convert NAM into nicotinic acid which re-fuels the Pries-Handler pathway. (All information from this section comes from Lee *et al.*, 2020³⁰.)

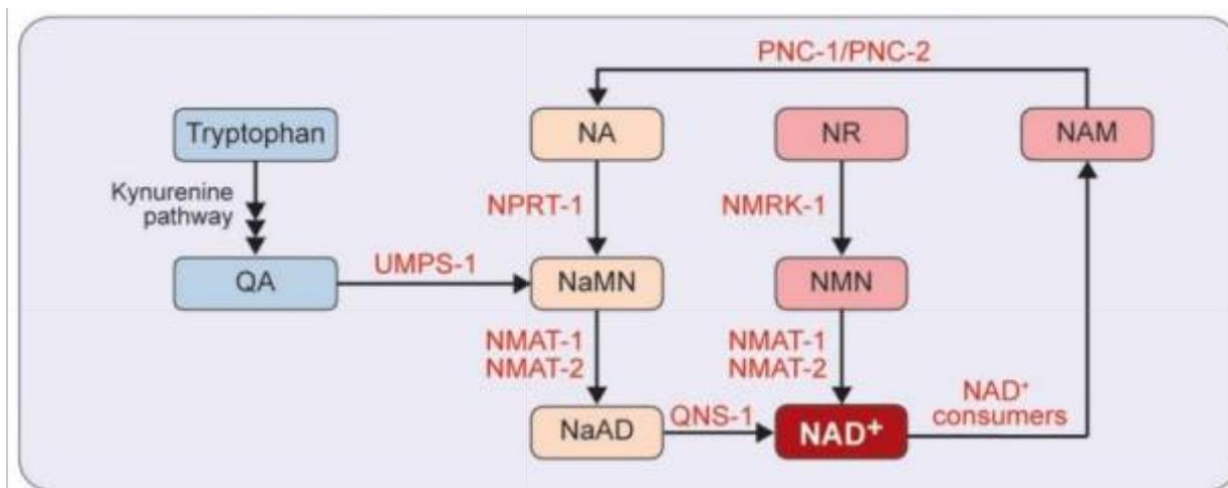


Figure 4: NAD^+ Metabolism

Figure modified from Lee *et al.* 2020³⁰

SARM1/TIR-1 NAD⁺ Consumption

Although SARM1 in humans and TIR-1 in *C. elegans* exhibit opposite effects on the immune system, they function identically in several key ways: they both localize to the axon where they enact stress-mediated NAD⁺ depletion and axon destruction. While I study the toll of TIR-1 on unstressed animals, future research could examine how stress modulates TIR-1's impact, particularly to see if this normally destructive gene plays a protective role during stress—a hypothesis that would explain why SARM1/TIR-1 is so evolutionarily conserved.

A Brief SARM1 History

In 1850, Dr. Augustus Waller observed that when he sliced or crushed a neuron, the distal branch of the neuron fragmented and then disintegrated within two days³¹. For over a century, doctors assumed that this process of “Wallerian degeneration” occurred passively, through simple necrosis. In 1989, a mutant strain of mouse whose neurons remained intact for over two weeks post-axotomy challenged the prevailing belief³¹.

Usually NMNAT1—the enzyme responsible for converting NMN to NAD⁺—localizes to the nucleus while NMNAT2 acts in the cytosol³¹. In mutant mouse strain, NMNAT1 erroneously localized to the cytosol. Following nerve injury, cytosolic NAD⁺ levels typically plummet, but in the mutants, NMNAT1 supported NMNAT2 by maintaining the cytosolic pool of NAD⁺³¹.

By 2012, researchers identified SARM in a forward genetic screen for other mutations that protect against Wallerian degeneration³². Like strains with mislocalized NMNAT1, SARM knockouts maintain cytosolic NAD⁺ levels post-axotomy. When scientists observed that axotomy disrupts NMNAT2 transport to the distal portion of the axon the finding clarified a tug-of-war model for the survival of the distal axon: while NMNAT2 offers salvation by replenishing cytosolic NAD⁺ levels, SARM1 works to execute the neuron by depleting NAD⁺.

Axotomy disconnects NMNAT2 from the distal axon, but stressors more tolerable than axotomy still push the tug-of-war balance towards SARM1's favor. In intact neurons, oxidative stress will cause JNK to phosphorylate and upregulate SARM1's activity to overpower NMNAT2³³. Under conditions of ischemia and glucose-deprivation, JNK association likely also plays a role in helping SARM1 prevail against its competitor³⁴.

Interestingly, during Wallerian degeneration, SARM1 promotes degeneration in the distal axon while inhibiting regeneration in the proximal axon through two separate pathways³⁵. Perhaps SARM1 overreacts, executing neurons and preventing regeneration during stress that a neuron could recover from. But being so evolutionarily conserved, perhaps SARM1 carries out a necessary role, sacrificing defective neurons for the benefit of the organism.

Mechanism of SARM1 activation

SARM1 senses its competitors' weakness by measuring the ratio between NMNAT's substrate and product. If NMNAT fails to convert NMN to NAD^+ , the NMN/NAD^+ ratio rises, triggering SARM1³⁶. The protein springs into action, cleaving NAD^+ and further driving the NMN/NAD^+ ratio to initiate a catastrophic feedback loop³⁶. An understudied second positive feedback loop may exist through a SARM1-induced MAPK cascade that activates JNKs³⁷. As NAD^+ levels in the neuron plummet, so do levels of ATP³⁷. Shortly thereafter, calpains—calcium-activated proteases—break down the axon³⁷. While the execution pathway requires further study, calpains may activate when ATP-dependent calcium pumps run out of fuel³⁷, because cADPR, a product of NAD^+ cleavage, opens calcium channels³⁸, or because of both.

Six SARM1 domains entwine together to prepare for moment NMNAT fails: a mitochondrial localization domain, two ARM domains which regulate autoinhibition, two SAM domains which regulate oligomerization, and a TIR domain which cleaves NAD^+ into NAM and ADPR or cADPR³⁹. Cryo-EM studies reveal that SARM1 oligomerizes into an eight-membered ring³⁹, wielding eight TIR domains like the teeth of a bear trap. SARM1 only cleaves NAD^+ when the TIR teeth snap shut to gain enzymatic activity³⁹.

In the inactive state, NAD^+ binds to the ARM autoinhibitory domains, pulling the TIR domains to the edge of the octameric ring³⁹. NMN fits in the ARM binding pocket with a higher affinity than NAD^+ ³⁶, but typically, NAD^+ outcompetes NMN because it exists at a higher concentration in the neuron³⁶. If the NMN/NAD^+ ratio rises (either by NAD^+ depletion, NMN supplementation,

or both) NMN saturates the ARM binding sites³⁶, snapping the bear trap shut. All eight of the TIR domains collapse to the center of the ring where they form homodimers and begin to catastrophically deplete local levels of NAD⁺³⁶.

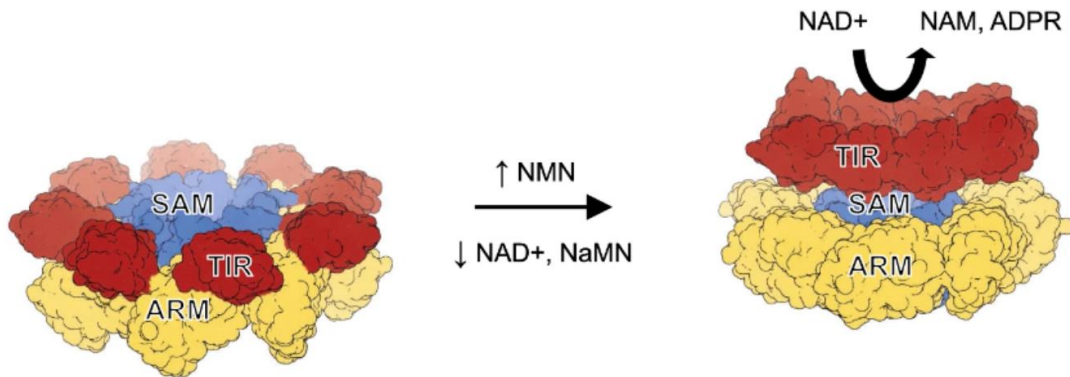


Figure 5: The SARM1 Bear Trap

Figure modified from Khazma *et al.* 2023⁴⁰

No studies examine how age-related NAD⁺ decline impacts SARM1 activity. Of course, the more NAD⁺ declines, the more precipitous SARM1's trigger becomes. Still, NAD⁺ levels in the brain decline by about 10-25% with age⁴¹ while a neuron's NMN/NAD⁺ ratio must increase nearly ten-fold to trigger SARM1 activation³⁶. Age-related stressors other than NAD⁺ decline may also work to push the SARM1 trigger.

TIR-1 Stress Mediation

TIR-1 shares 60% homology with over 85% of the SARM1 sequence³⁵. The two are highly conserved, and indeed, share many functions. Unlike SARM1, TIR-1 activation upregulates

innate immune response genes in the intestine²³. Like SARM1, TIR-1 activates under stress. Infection²³, cholesterol deficiency²³, oxidative stress⁴², and anoxia⁴³, all trigger TIR-1 multimerization, NAD⁺ cleavage, and immune cascade pathways. By coupling genes that respond to stressors and genes that respond to infection under the same signaling cascades, TIR-1 allows *C. elegans* to preemptively ward off infection when the worm is most vulnerable.

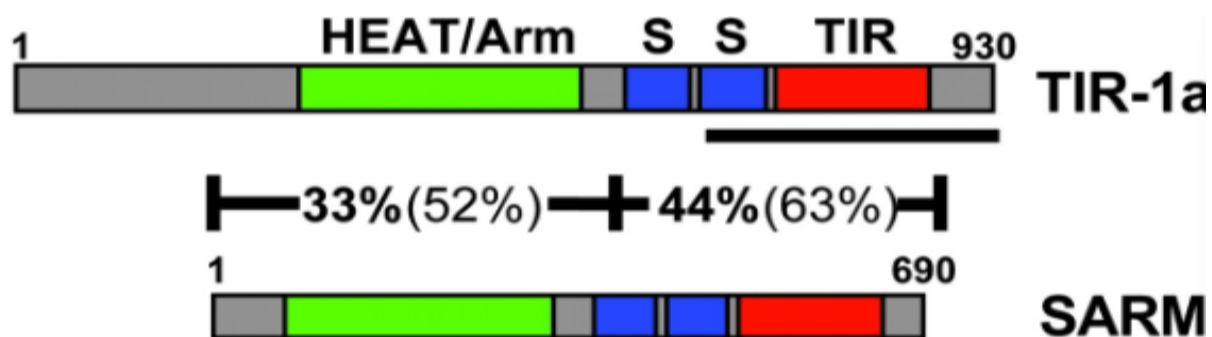


Figure 6: TIR-1 and SARM1 Sequence Similarity

The bold numbers indicate percent of identical amino acids while the non-bolded numbers indicate homology. Figure modified from Liberati *et al.* 2004⁴⁴

TIR-1 also regulates neuronal death but does so less efficiently than SARM1. A single slice through a *C. elegans* neuron fails to induce Wallerian degeneration⁴⁵. Instead, the neuron must suffer double axotomy for TIR-1 to promote the degeneration of the middle fragment while inhibiting regeneration in the rest of the axon³⁵. Even then the effects are modest; in TIR-1 mutant worms, double axotomy results in only 18% less degeneration³⁵. In vitro studies suggest that TIR-1 fails to assemble as stably as SARM1, usually forming a nonamer rather than an octamer⁴⁵. The oligomerization renders the protein constitutively active yet weak—NMN and NAD⁺ fail to regulate its enzymatic activity, and TIR-1 works inefficiently with a K_m roughly ten-fold greater than SARM1's⁴⁵.

Conclusion

Across species, NAD⁺ regulates nearly all biological processes; it is fundamental to life.

Understanding how lifeforms process NAD⁺, and especially how the process fails with age, sheds light on life's fragility, its constant reliance on a machine of metabolic pathways depleting and replenishing to fuel existence.

Current research claims that targeting the novel NAD⁺-consumer SARM1/TIR-1 poses only the beneficial effect of neuroprotection, with no disruption to the fragile metabolic web. My research refutes this claim. By studying TIR-1 mutant *C. elegans*, I examine the toll of TIR-1 on longevity, reproductive health, and the metabolome, to create a more holistic picture of NAD-consumption. This work informs aging populations of the interconnectedness between stress, health, metabolic decline, and longevity, working to understand how better aging requires more than cure-all therapeutics.

Chapter 2

Materials and Methods

C. elegans Strains and Maintenance

All *C. elegans* strains grew on NGM agar spotted with 250 μ L of *E. coli* OP50. An incubator kept the worms at 20° Celsius. If a generation of worms starved, three generations of their progeny were maintained before resuming experimentation. Six strains of worms were studied, all obtained from the Caenorhabditis Genetics Center: N2 (wildtype), IG685 (*tm3036*), RB1085 (*ok1052*), RB2145 (*ok2859*), VC526 (*gk264*), and ZD101 (*qdl4*).

Brood Size Assays and Lifespan Assays

To sync the worms, several adults were allowed to lay eggs for one hour, after which the adults were removed from the plate. When the progeny reached L4, they were placed on new plates, each animal receiving its own plate. When the L4 worm developed into an egg-laying adult, the animal was transferred to a fresh plate daily. After each transfer, the brood-size on the old plate was counted. Once the parent worm stopped laying eggs, it was no longer transferred to new plates. Instead, it was assessed for survival each day. Survival was assessed by prodding the animal with a platinum wire; movement confirmed life, no movement confirmed death. Worms that went missing or internally hatched were censored.

Multigenerational Live-Food Metabolomics

20-25 plates of worms were cultivated for each strain. The worms were collected from plates when they had eaten nearly all of the food on the plate but had not yet starved. The worms were then extracted in 40:40:20 Acetonitrile:Methanol:H₂O + 0.5% Formic Acid + 17.8 w/v Ammonium Bicarbonate to neutralize the formic acid. The lab owns and operates its own LC-MS system with the support of the Huck Metabolomics Core Facility. The LC-MS method is based on hydrophilic interaction chromatography (HILIC) coupled to an Orbitrap Exploris 240 mass spectrometer. Raw LC-MS data were converted to mzXML format using the command line “msconvert” utility, and the data was analyzed via the EL-MAVEN software version 12. Protein concentrations were determined via BCA and used to normalize the total ion counts.

Data Analysis

All graphs other than the correlation plots were created with GraphPad Prism. The statistical significance symbols indicate the following:

- ns – $P > 0.05$
- * - $P \leq 0.05$
- ** - $P \leq 0.01$
- *** - $P \leq 0.001$
- **** - $P \leq 0.0001$

Chapter 3

Results

The Effect of TIR-1 on Longevity

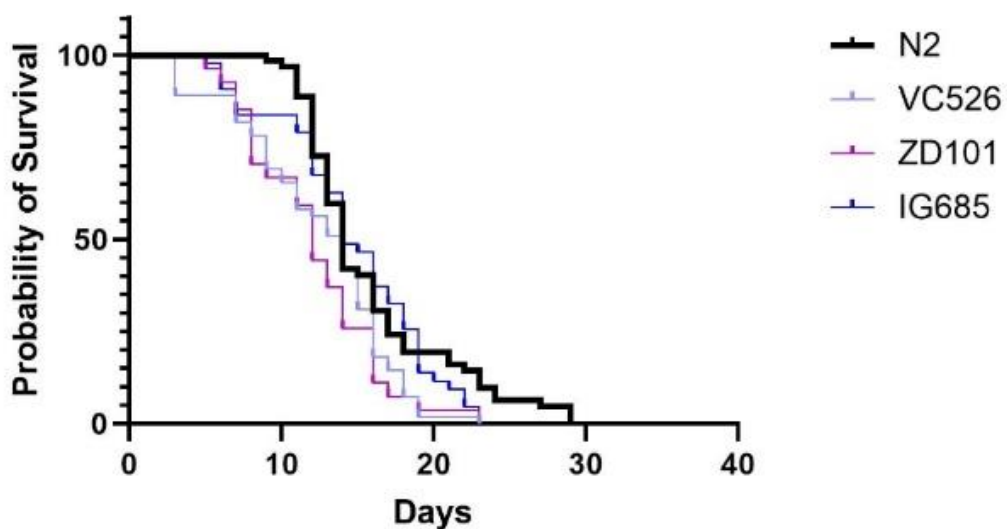
Wu *et al* previously concluded that the lifespans of three TIR-1 mutant strains—IG685, RB1085, and ZD101—are identical to the wild-type control strain, N2⁴⁶. To verify her data and to determine if TIR-1 impacts longevity, I conducted lifespan assays on the three strains Wu studied and two other TIR-1 mutant strains—RB2145 and VC526— available from the Caenorhabditis Genetics Center.

For four strains, N2, IG685, VC526, and ZD101, I conducted three biological replicates, tracking the lifespan of 70 animals from each strain in total. For the remaining two strains, RB1085 and RB2145, I only had the time to conduct a single biological replicate, studying thirty animals from each strain. If animals crawled off a plate or internally hatched (the term for when eggs hatch within the parent's body), I excluded their data.

Figure 7 depicts Kaplan-Meier survival curves of the mutant TIR-1 strains, demonstrating that TIR-1 mutations impact the probability of survival in all strains except for IG685. Strains VC526, ZD101, and RB2145 have a lower probability of survival at any given time point compared to N2, while the strain RB1085 has a greater probability of survival. Though a Mantel-Cox test confirms a statistically significant difference in the mutant survival curves compared to the wild-type strain, my data may not conflict with Wu's.

Kaplan-Meier Survival Curves

A



B

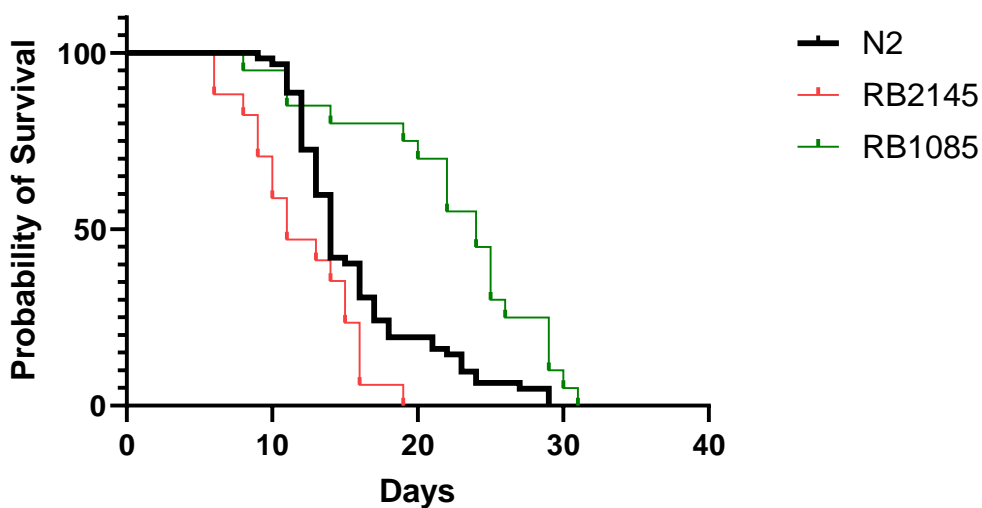


Figure 7: Kaplan-Meier Survival Curves of TIR-1 Mutants Compared to N2

- (A) Survival curve displaying pooled values from three independent experiments, no significance in IG685 (n=43), $p < 0.01$ for VC526 (n=55) and ZD101 (n=27), Log Rank (Mantel-Cox) test
- (B) Survival curve displaying pooled values from three independent experiments for N2 (n=62), and values from a single experiment in RB1085 (n=20) and RB2145 (n=17), $p < 0.01$ for RB2145, $p < 0.001$ for RB1085, Log Rank (Mantel-Cox) test

Kaplan-Meier curves indicate the probability of surviving a short time-interval, not necessarily the probability of surviving into old age. In other words, two strains may share an average lifespan while dying at different frequencies at each stage of life. To visualize the frequency of death at different ages, I superimposed Gaussian distributions over frequency plots that graph the number of worms that died on a given day, shown in Figure 8.

Frequency Plots of Worm Lifespan

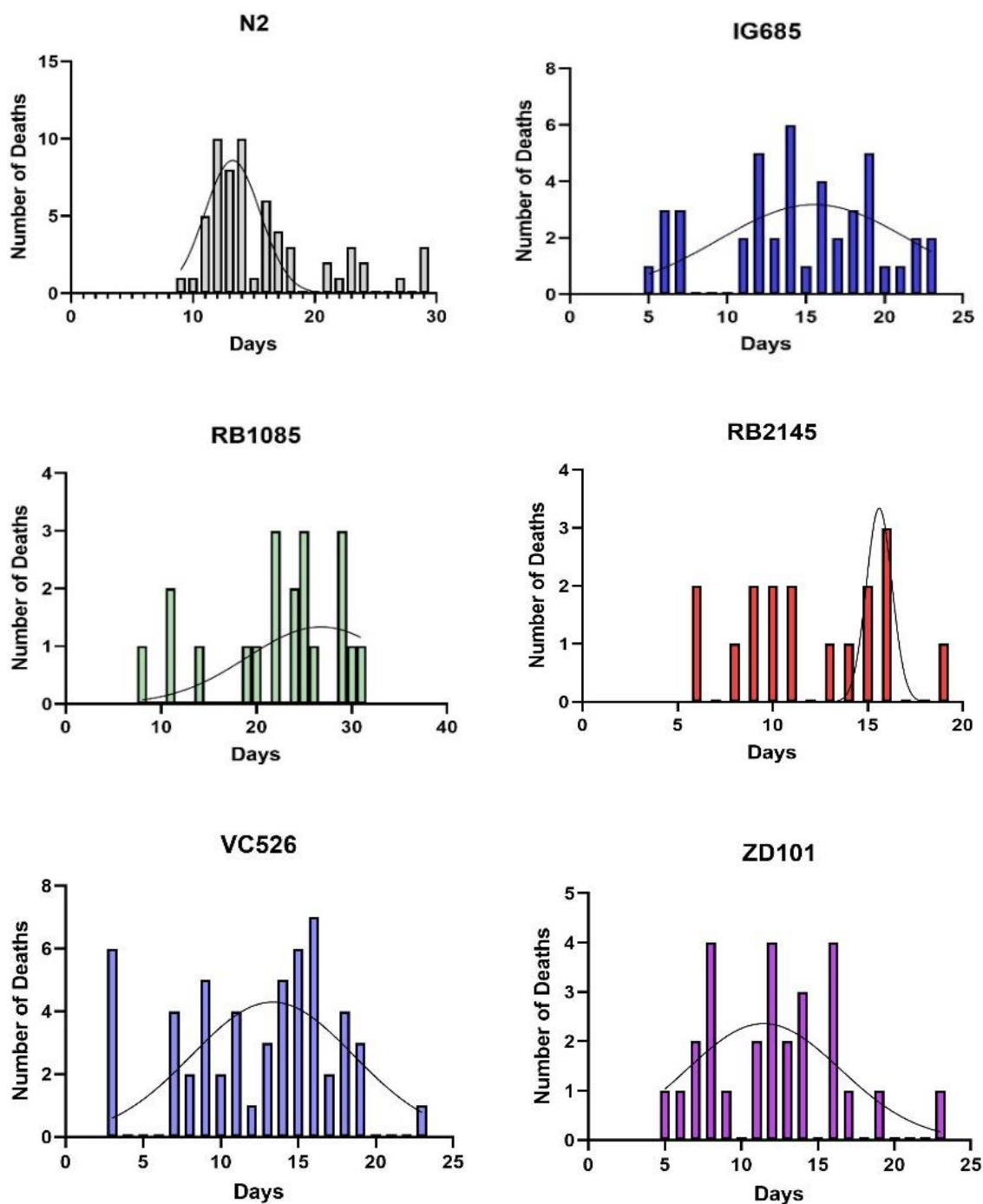


Figure 8: Gaussian Distributions of Strain Longevity

The distribution of lifespans in N2 worms differs from the TIR-1 mutant strains, corresponding to the statistical significance in the difference between Kaplan-Meier survival curves

Indeed, while the Gaussian distributions for each strain of worm varies, the ANOVA test comparing biological replicate averages determined no statistical significance in longevity (Figure 9). However, if I increase the statistical power by treating each worm as a biological replicate, the lifespan data corroborates the Kaplan-Meir survival curve data: in all strains except IG685, the mutation impacts longevity.

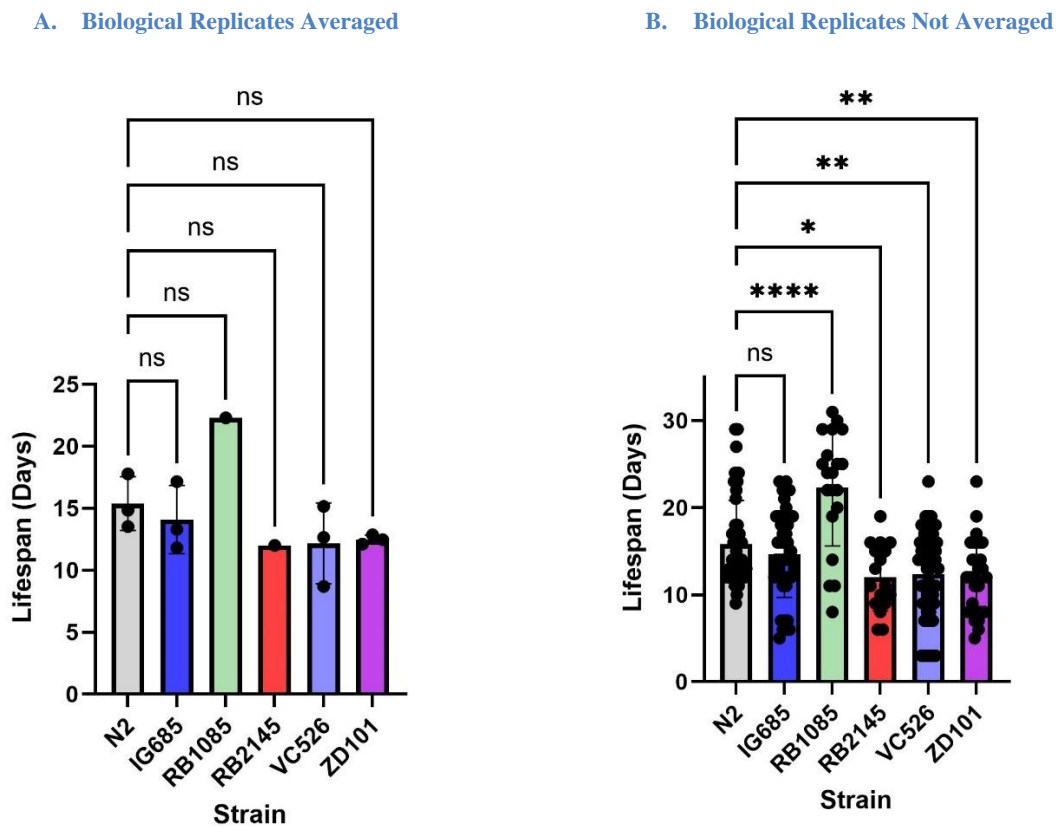


Figure 9: Average Longevity of TIR-1 Mutant Strains Compared to N2

- (A) When data from each biological replicate is averaged, the change in longevity is not statistically significant in any TIR-1 mutant compared to N2, one-way ANOVA
- (B) When data from each replicate is pooled, the statistical power increases, and all strains except for IG685 significantly differ in their longevities compared to N2. RB1085 is the only strain where longevity increases, one-way ANOVA

The Effect of TIR-1 on Reproductive Health

My data suggests that TIR-1 modifies the probability of survival at different life stages. By measuring the brood sizes of my strains, I characterize health during childbirth, the most taxing phase of a worm's lifespan. I counted the brood size of N2 and VC526 worms four separate times, and the brood sizes of IG685 and ZD101 three separate times, with 10-20 animals per trial.

As in the longevity assay, the number of worms counted as a biological replicate determine the statistical power of the brood assay. Figure 10 shows the downtrend in brood size for each of the strains compared to N2. When plotting the brood size of each worm, the data is statistically significant for all strains, while the data is only statistically significant for ZD101 when plotting the average of each biological replicate.

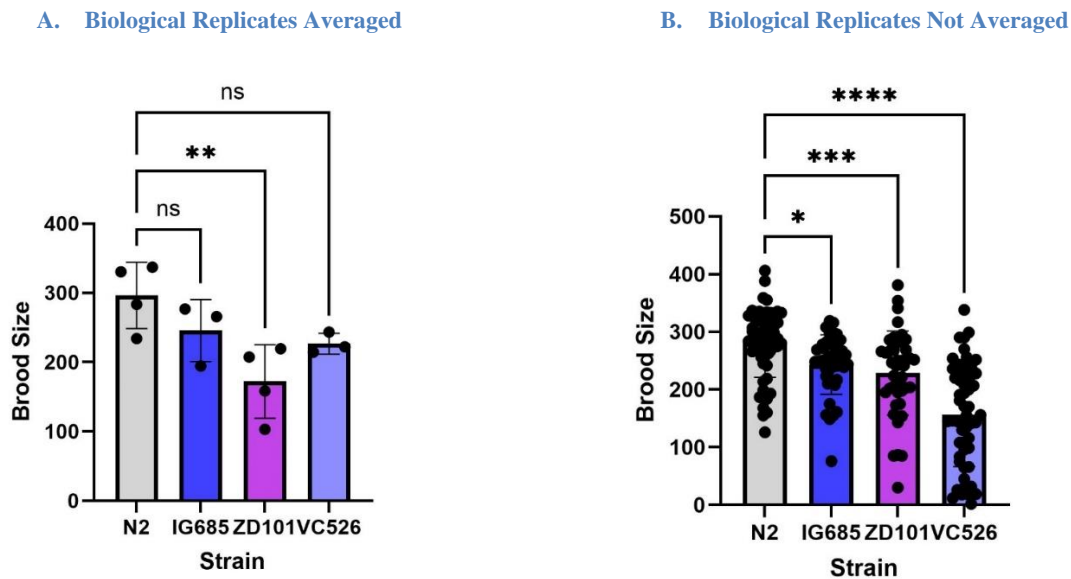


Figure 10: Brood-Size of TIR-1 Mutant Strains Compared to N2

- (A) When data from each biological replicate is averaged, the change in brood-size is not statistically significant in any TIR-1 mutant compared to N2, one-way ANOVA, outliers removed
- (B) When data from each replicate is pooled, the statistical power increases, and all strains demonstrate a significant decline in brood-size compared to N2, one-way ANOVA, outliers removed

When I conducted the brood-size assay, I excluded data from worms that internally hatched before day five of adulthood; these worms died before laying their full brood-size. However, I discovered that TIR-1 mutant worms internally hatch more frequently. I recorded the percentage of worms that internally hatched in my brood-size trials, and I also recorded the data for the RB1085 and RB2145 strains while I conducted their longevity assay. As depicted in Figure 11, internal hatching increased statistically significantly in strains IG685, ZD101 and RB2145, as determined by an unpaired, two-tailed t-test.

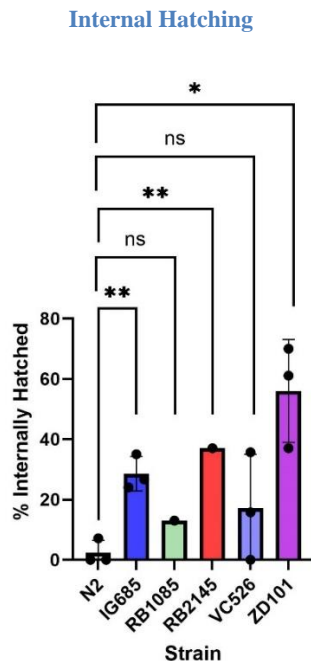


Figure 11: Percent of Worms that Internally Hatch

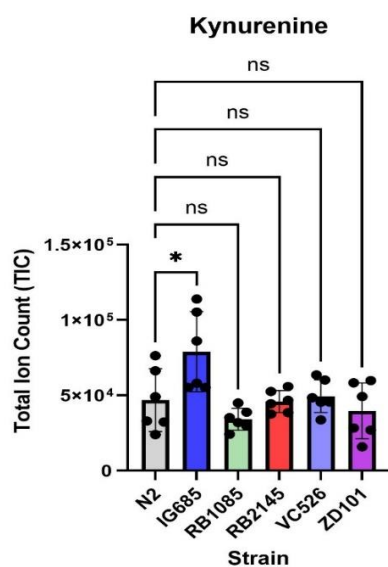
Compared to N2 (n=20, 15, 28), internal hatching increases in IG685 (n=20, 15, 25), RB2145 (n=27), and ZD101 (n=20, 18, 27) while trending upwards in RB1085 (n=23) and VC526 (n=20, 19, 28), unpaired two-tailed t-test

The Effect of TIR-1 on NAD⁺ Metabolism

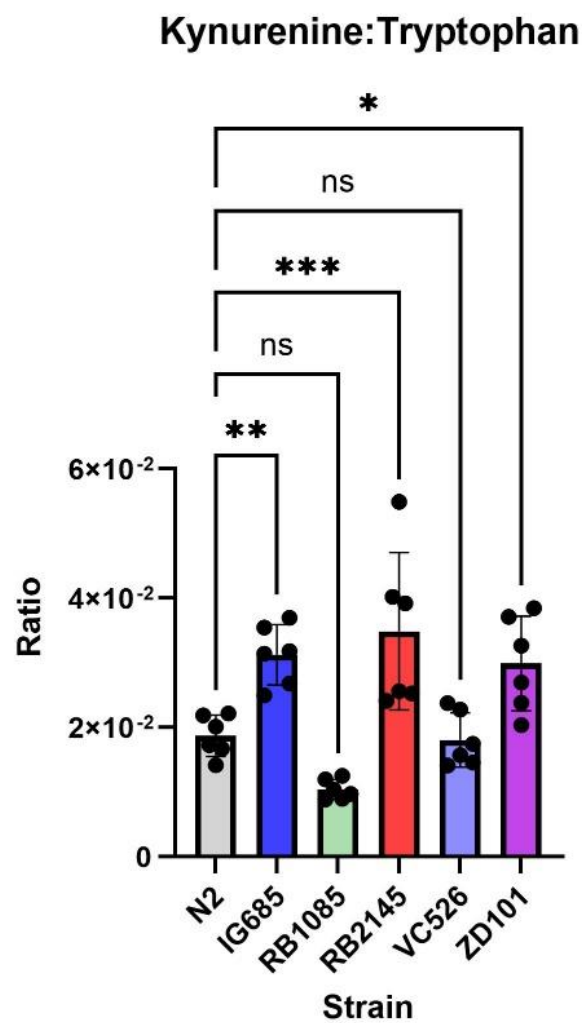
Role of TIR-1 in the *De Novo* Pathway

To understand how TIR-1 affects tryptophan entering the *de novo* pathway, I compared the total ion counts of metabolites from the *de novo* path in the mutant strains versus the N2 strain. While there is no statistical significance in the amount of tryptophan between strains, there is a marked increase in kynurenine in strain IG685 (Figure 12). When normalized for tryptophan, the kynurenine:tryptophan ratio reveals that in addition to IG685, strains RB2145 and ZD101 maintain relatively high levels of kynurenine.

A



C



B

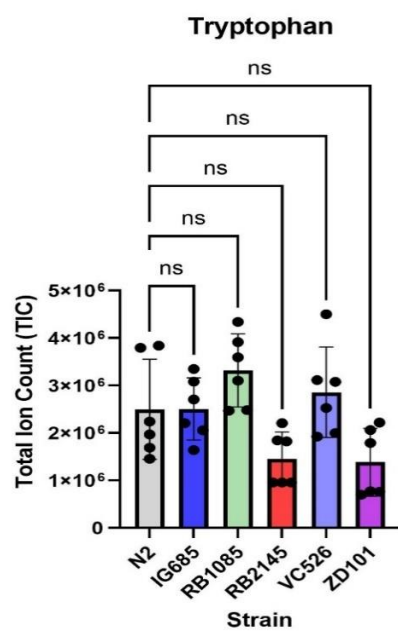


Figure 12: Comparison of Kynurenine and Tryptophan Levels Across TIR-1 Mutant Strains

(A) Kynurenine's total ion count increases in IG685, one way ANOVA

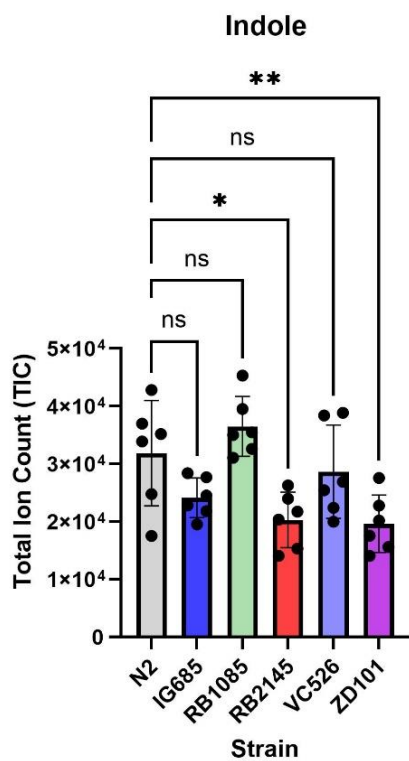
(B) Tryptophan's total ion count does not significantly change in any mutant strain, one-way ANOVA

(C) A higher-than-normal ratio of tryptophan converts into kynurenine in strains IG685, RB2145, and ZD101, one-way ANOVA

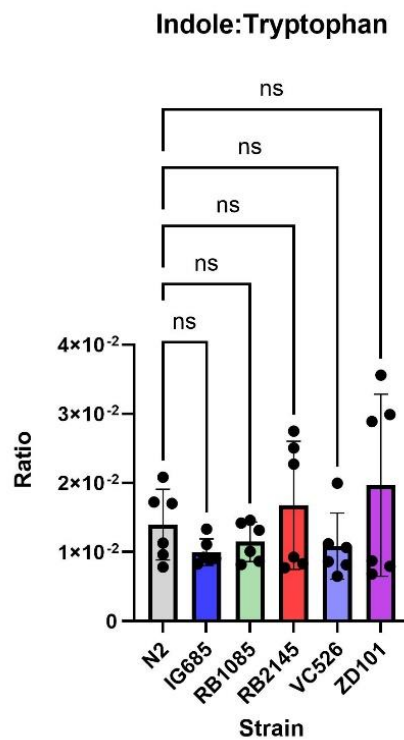
To understand if kynurenine consumption is low or if kynurenine synthesis from tryptophan is high, I searched for metabolites in other tryptophan pathways, and for metabolites further down the *de novo* path. I obtained readouts for two metabolites in the indole pathway, tryptamine and indole, and one metabolite further down the *de novo* path, 3-hydroxyanthranilic acid

The same three strains with elevated kynurenine lacked tryptamine to a statistically significant degree. The same pattern existed for indole, where the total ion count dropped in RB2147 and ZD101, with levels trending downward in IG685. However, once normalized by the level of tryptophan, the differences are not statistically significant (Figure 13).

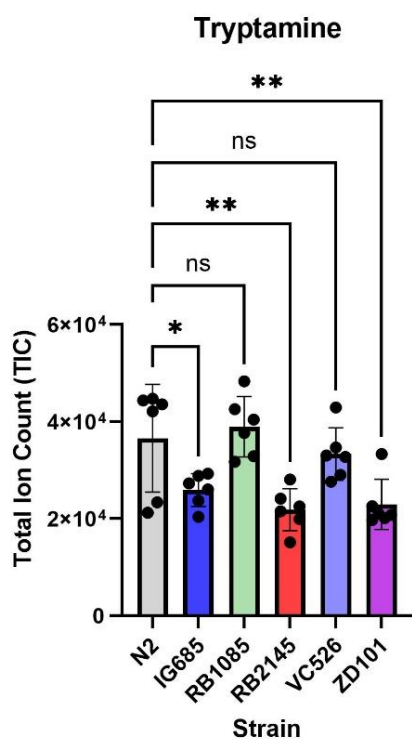
A



B



C



D

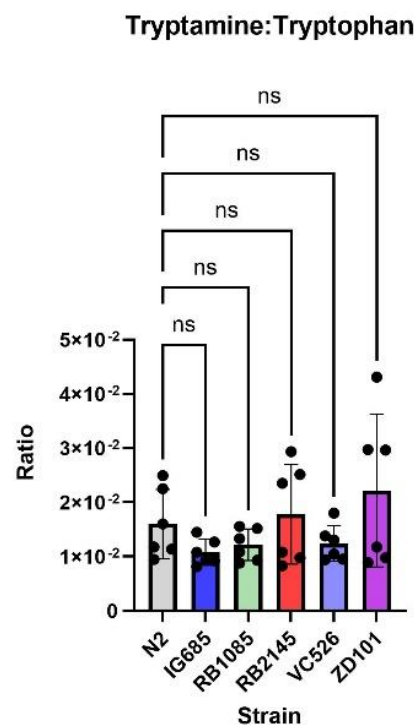


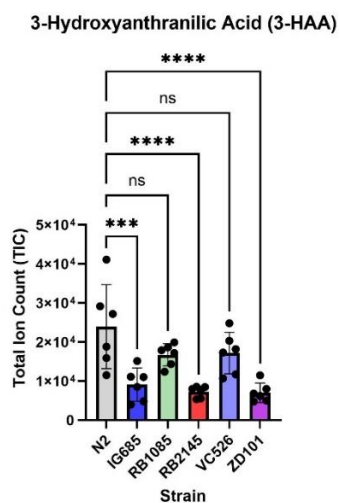
Figure 13: Comparison of Indole Pathway Metabolites Across TIR-1 Mutant Strains

- (A) Indole's total ion count decreases in RB2145 and ZD101, one way ANOVA
- (B) Tryptophan to indole turnover does not change in the TIR-1 mutants, one way ANOVA
- (C) Tryptamine's total ion count decreases in RB2145 and ZD101, one way ANOVA
- (D) Tryptophan to tryptamine turnover does not change in the TIR-1 mutants, one way ANOVA

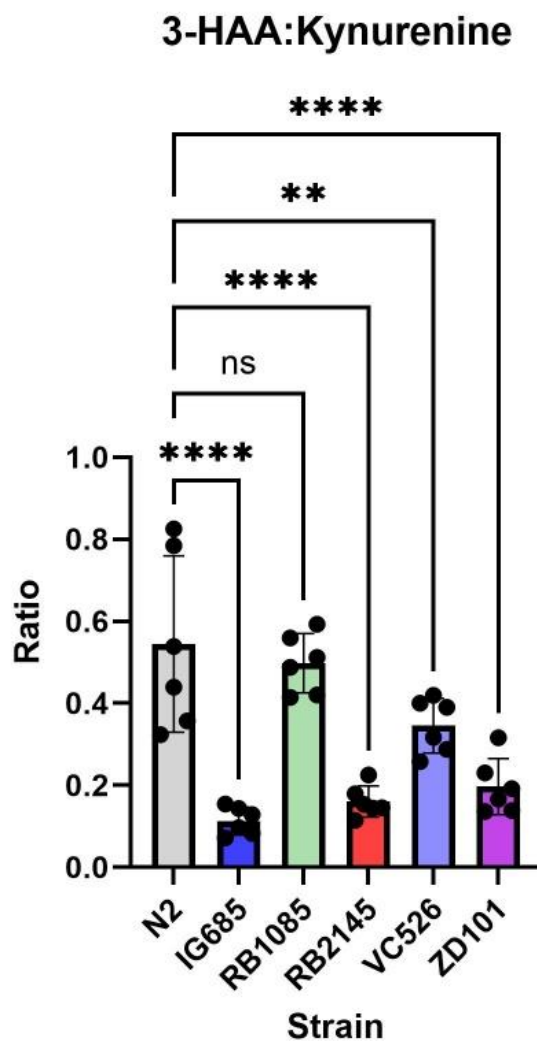
Though kynurenine levels remain even across strains, even increasing in IG685, levels of 3-hydroxyanthranilic acid decrease in IG685, RB2145, and ZD101 (Figure 14). To see if kynurenine shunted out of the *de novo* pathway, I searched for kynurenic acid, anthranilic acid, and xanthurenic acid—all of the possible metabolites that the *de novo* pathway siphons into while kynurenine converts to 3-hydroxyanthranilic acid. The LC-MS did not resolve peaks for any of the metabolites.

Instead, I calculated the 3-hydroxyanthranilic acid:kynurenine ratio to determine if, compared to the N2 strain, the mutants converted less kynurenine into 3-hydroxyanthranilic acid. Figure 14 demonstrates a reduced conversion rate in all but one mutant strain.

A



C



B

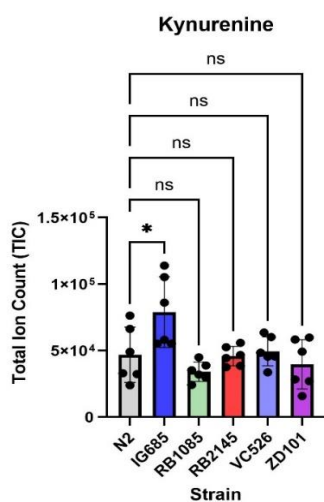


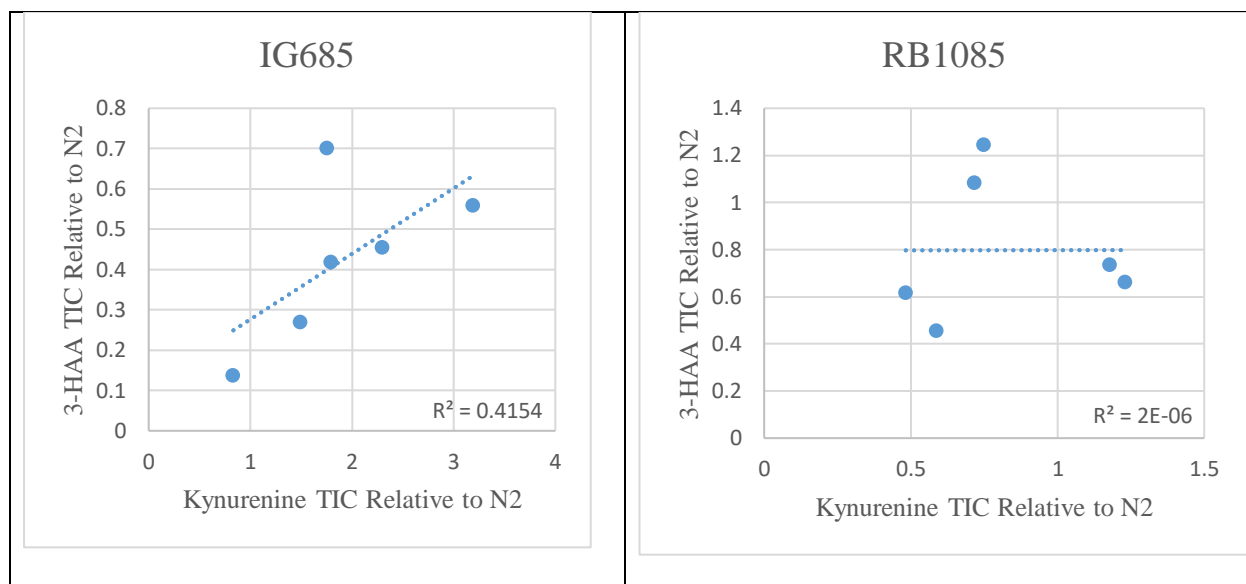
Figure 14: Comparison of Kynurenine and 3-Hydroxyanthranilic Acid Levels Across TIR-1 Mutant Strains

(A) 3-Hydroxyanthranilic acid's total ion count decreased in IG685, RB2145, and ZD101, one way ANOVA

(B) Kynurenine's total ion count increases in IG685, one way ANOVA

(C) A lower-than-normal ratio of kynurenine converts into 3-hydroxyanthranilic acid in strains IG685, RB2145, VC526, and ZD101, one-way ANOVA

I then investigated the alternative hypothesis that one of the two enzymes involved in converting kynurenine into 3-hydroxyanthranilic acid downregulates in TIR-1 mutants. In each strain, I calculated the degree to which kynurenine's total ion count (TIC) deviated from the N2 strain. I then calculated how much the 3-hydroxyanthranilic acid TIC deviated from N2. To determine if the fold change in kynurenine correlated to fold change in 3-hydroxyanthranilic acid, I plotted the values and determined the r^2 value, as depicted in Figure 15. With an average r^2 value of 0.19, the normalized kynurenine levels failed to correlate with the normalized 3-hydroxyanthranilic acid levels.



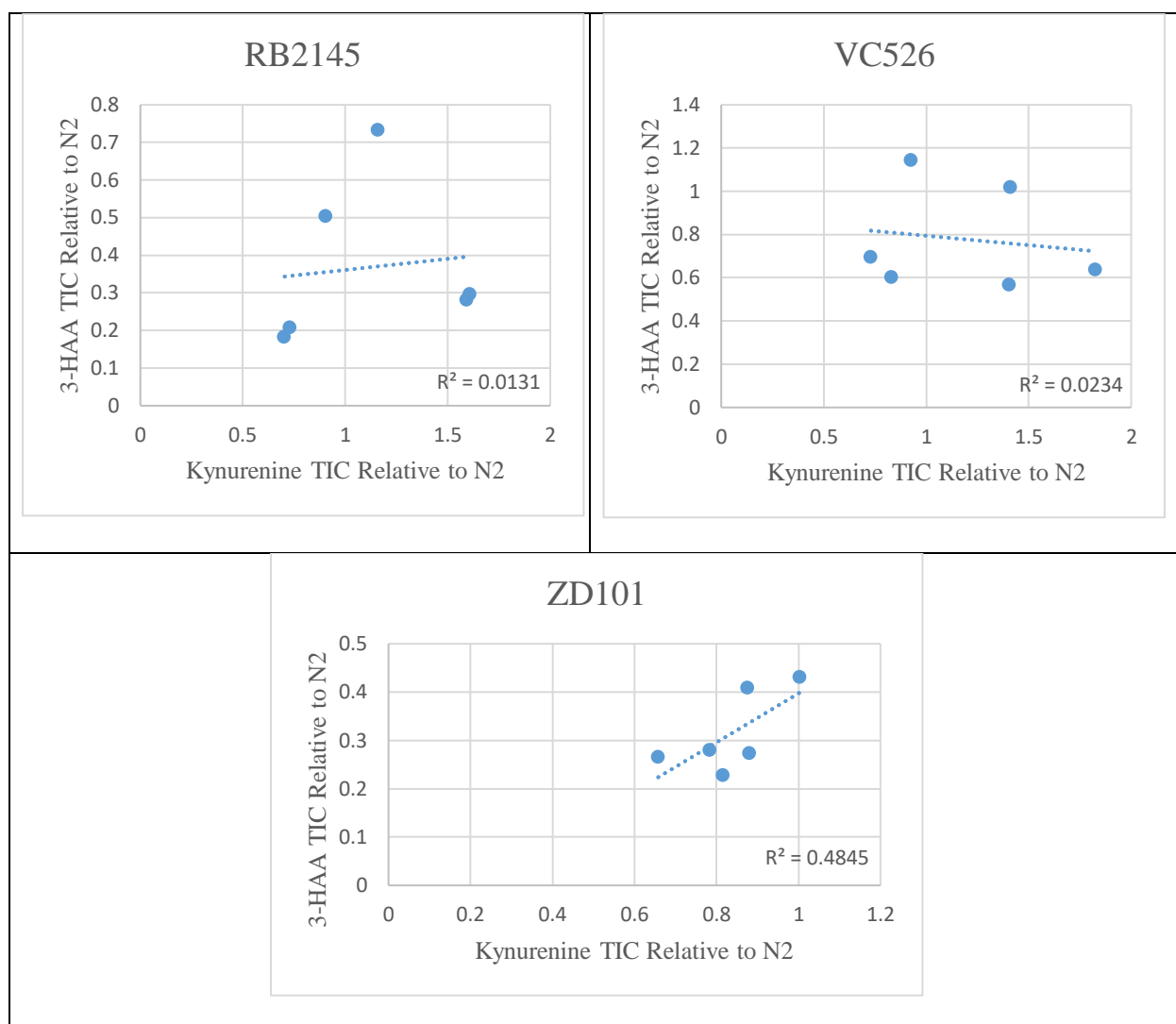


Figure 15: Correlation Between the Fold Change in Kynurenine and the Fold Change in 3-Hydroxyanthranilic Acid

Little correlation exists in any of the strains between the change in kynurenine and the change in 3-hydroxyanthranilic acid

In two enzymatic steps, 3-hydroxyanthranilic acid converts into NaMN, which feeds into the Pries-Handler pathway. Despite the low 3-hydroxyanthranilic acid levels, NaMN remains statistically even across the board (Figure 16).

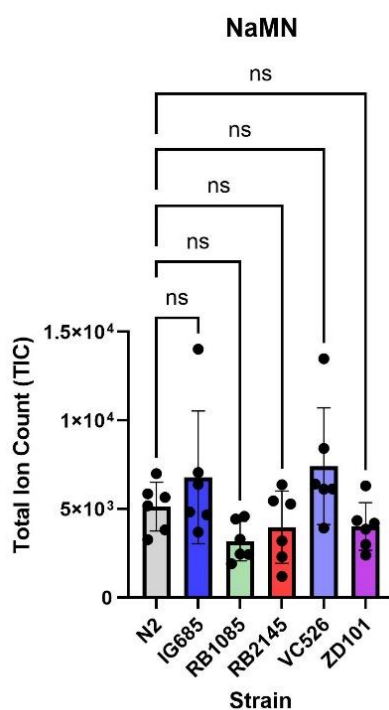


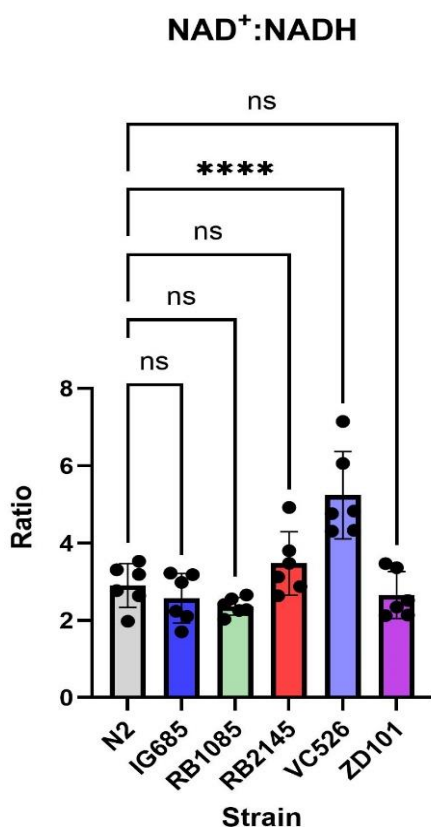
Figure 16: NaMN Total Ion Count in TIR-1 Mutant Strains

Though the NaMN total ion count trends downwards in strains RB1085, RB2145, and ZD101, none of the mutant strains depart from N2 with statistical significance, one-way ANOVA

Role of TIR-1 in Redox States

Because 3-hydroxyanthranilic acid functions as an antioxidant with decline implicated in brain injury⁴⁷, I searched for antioxidant-oxidant pairs to explore how TIR-1 affects redox states in an organism. I obtained readouts for two potent redox pairs, NAD⁺/NADH and glutathione disulfide/glutathione. In accordance with the decline in the 3-hydroxyanthranilic antioxidant, both pairs demonstrated a shift towards the oxidized state (Figure 17).

A



B

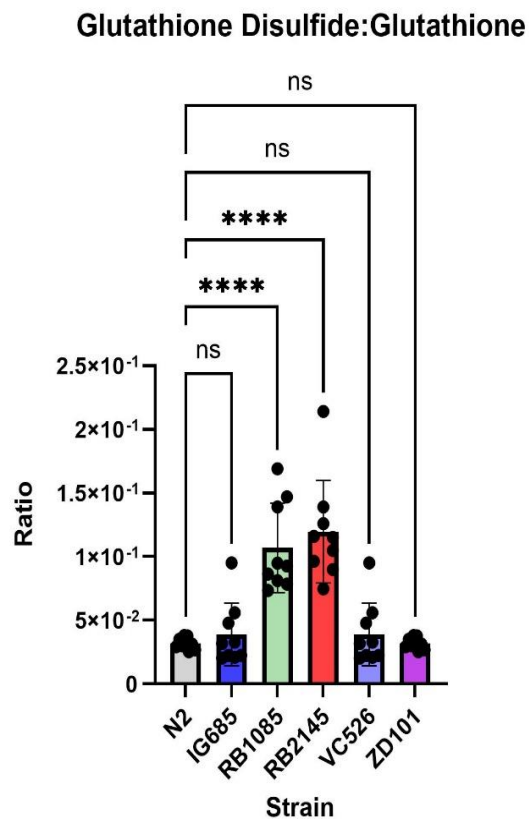


Figure 17: Comparison of Redox Couples Between TIR-1 Mutant Strains

(A) The NAD⁺:NADH ratio favors the oxidized species in strain VC526, one-way ANOVA

(B) The glutathione disulfide:glutathione ratio favors the oxidized species in strains RB1085 and RB2145, one-way ANOVA

Role of TIR-1 in NR Homeostasis

Although I expected that the TIR-1 mutant strains would consume less NAD⁺, the LC-MS data revealed that in strains RB1085, RB2145, and ZD101, NAD⁺ levels declined roughly 50% compared to the wild-type strain. Only VC526 trended towards an increase in NAD⁺, though not enough for statistical significance (Figure 18). Because the TIR-1 mutants showed no significant

change in NaMN, and I did not find a readout for NaAD, I looked to the NR \rightarrow NMN \rightarrow NAD⁺ pathway to understand how NAD⁺ precursors in the NR pathway contribute to NAD⁺ decline.

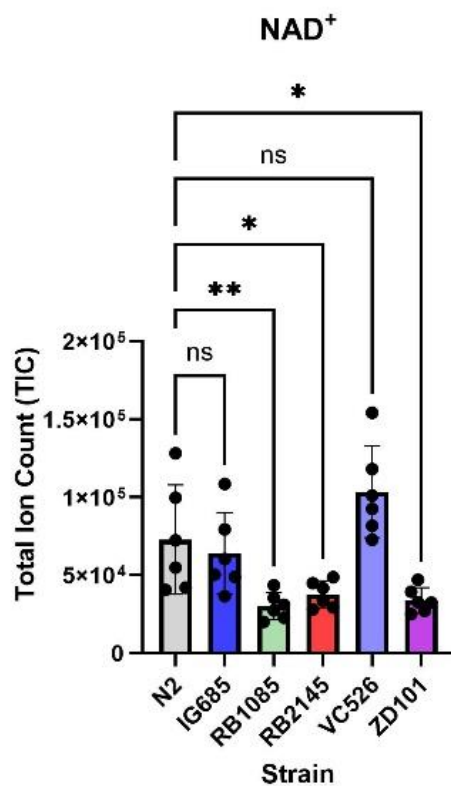
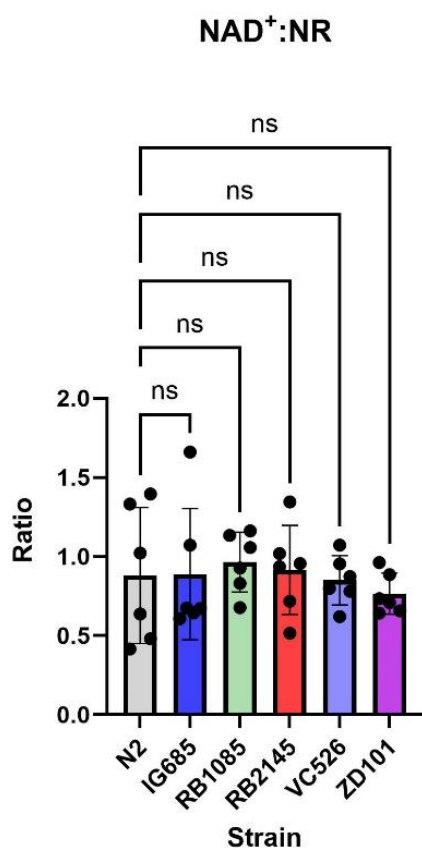


Figure 18: NAD⁺ Total Ion Count in TIR-1 Mutant Strains

The NAD⁺ total ion count decreases in strains RB1085, RB2145, and ZD101 while trending upwards in strain VC526, one-way ANOVA

Both NR and NMN showed the same pattern as NAD⁺—declining levels in RB1085, RB2145, and ZD101 with high levels in VC526. Tellingly, NR levels declined by roughly 50% in the same three strains that declined by roughly 50% in NAD⁺. When normalized against NR, the NMN:NR and NAD:NR ratios show no change across strains (Figure 19).

A



B

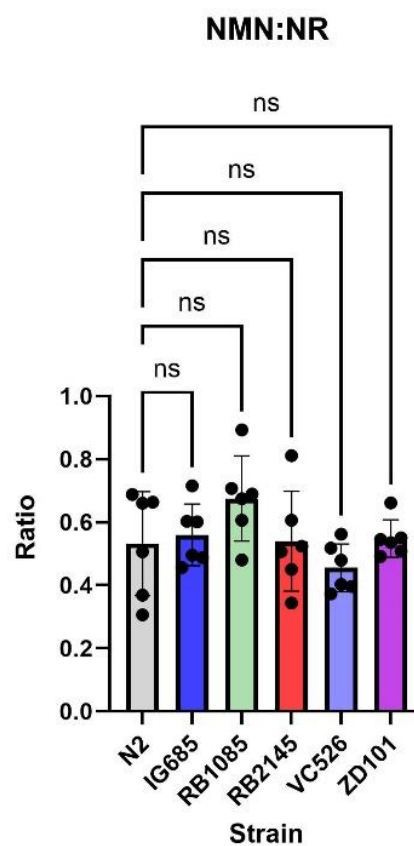


Figure 19: Metabolites of the NR Pathway Normalized to NR

(A) NAD⁺ levels change proportionally to NR levels in each of the TIR-1 mutant strains, one-way ANOVA

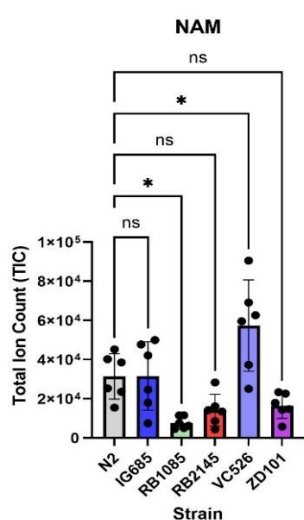
(B) NMN levels change proportionally to NR levels in each of the TIR-1 mutant strains, one-way ANOVA

Role of TIR-1 in NAD⁺ Consumption

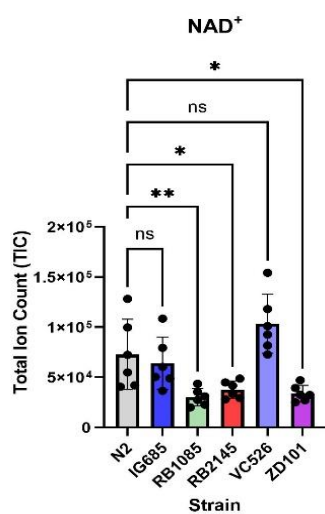
All NAD⁺ consumers break NAD⁺ into NAM. TIR-1 breaks NAD⁺ into NAM and ADPR, which in turn breaks down into AMP and ribose 5-phosphate. To understand the extent of TIR-1's role in NAD⁺ consumption, I searched for each of these metabolites.

In the mutants, I expected lower NAM, and it did decline in RB2145 while trending down in RB1085 and ZD101 (Figure 20). Perplexingly, NAM trended upwards in VC526, which prompted me to compare the levels of NAM against the levels of NAD^+ . I plot the NAM: NAD^+ ratio in Figure 20, where once normalized, there is no statistically significant difference in NAM levels, though in RB1085 and RB2145, the levels do trend down.

A



B



C

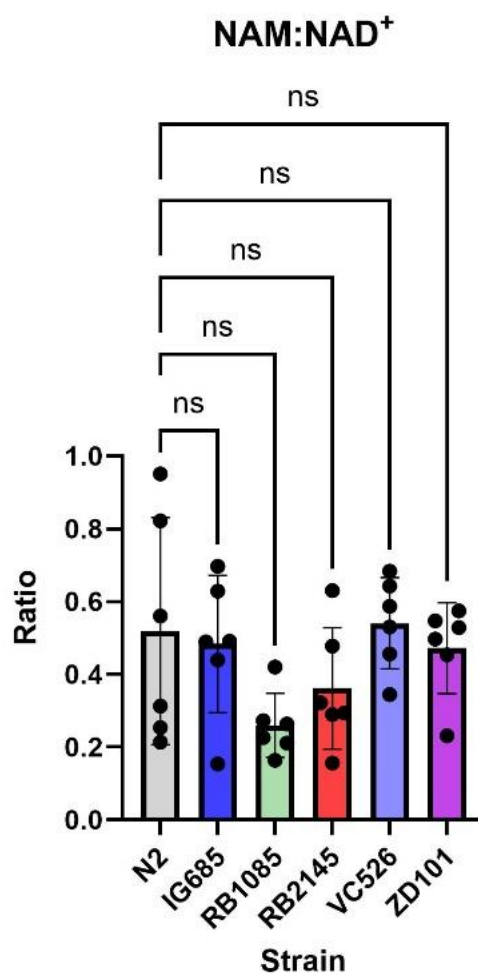
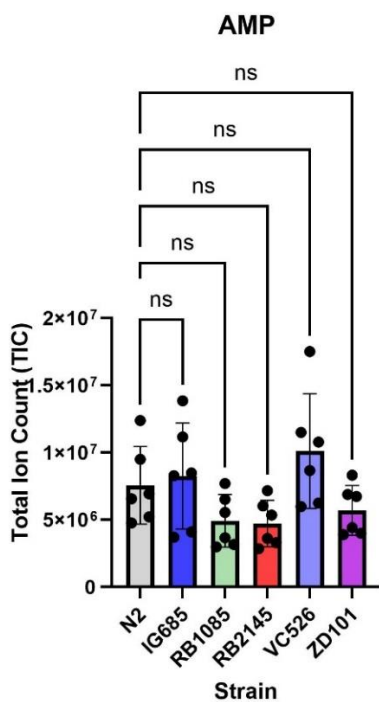


Figure 20: Comparison of NAM and NAD^+ Levels Across TIR-1 Mutant Strains

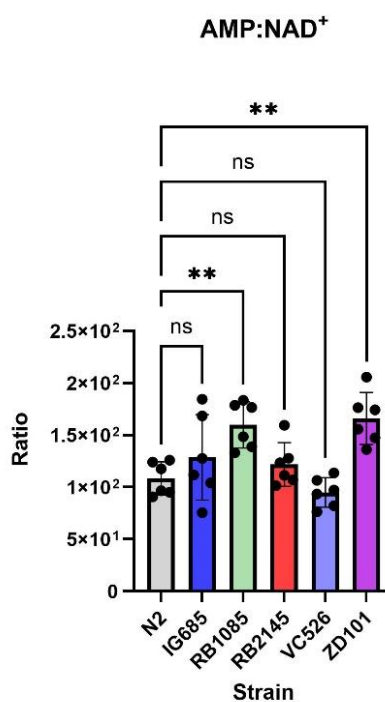
- (A) NAM's total ion count decreased in strain RB1085 and increased in VC526, one-way ANOVA
- (B) NAD^+ 's total ion count decreased in strains RB1085, RB2145, and ZD101 while trending upwards in VC526, one-way ANOVA
- (C) NAD^+ to NAM turnover does not significantly change in the TIR-1 mutants, though it trends down in strains RB1085 and RB2145, one way ANOVA

Similarly, AMP and ribose 5-phosphate levels decline with statistical or biological significance in strains RB1085, RB2145, and VC526, but once normalized against the levels NAD^+ , the metabolites tell a less straightforward story (Figure 21). The ribose 5-phosphate: NAD^+ ratio remains even across the strains with a downward trend in VC526. Meanwhile, the AMP: NAD^+ ratio remains even across the strains except for a statistically significant increase in strains RB1085 and ZD101.

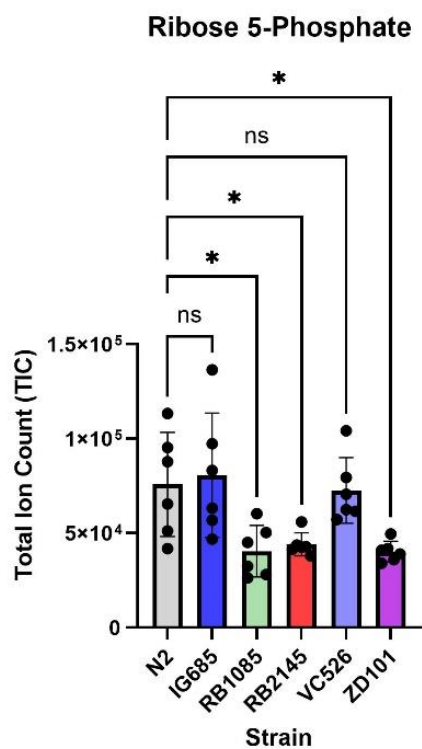
A



B



C



D

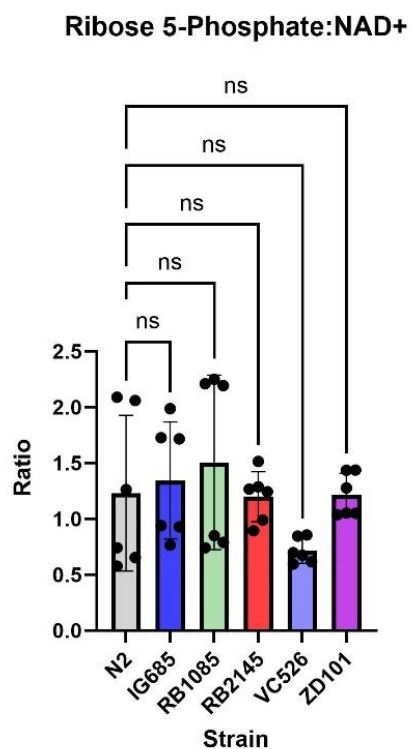


Figure 21: Comparison of ADPR Breakdown Metabolites Across TIR-1 Mutant Strains

- (A) AMP's total ion count does not significantly change in the TIR-1 mutants, though trends low in RB1085, RB2145, and ZD101, one way ANOVA
- (B) AMP levels normalized to NAD⁺ increase in strains RB1085 and ZD101, one-way ANOVA
- (C) Ribose 5-phosphate's total ion count decreases in strains RB1085, RB2145, and ZD101, one-way ANOVA
- (D) Ribose 5-phosphate levels normalized to NAD⁺ do not significantly change in any of the TIR-1 mutants, one-way ANOVA

Role of TIR-1 in the Salvage Pathway

To understand if TIR-1 impacts the salvage pathway, I determined the NA:NAM ratio for each strain. As depicted in Figure 22, the ratio indicates what proportion of NAM recycles back into

the Pries-Handler pathway. Though none of the ratios depart with statistical significance from the wild-type strain, the ratios in RB1085, RB2145, and ZD101 trend high.

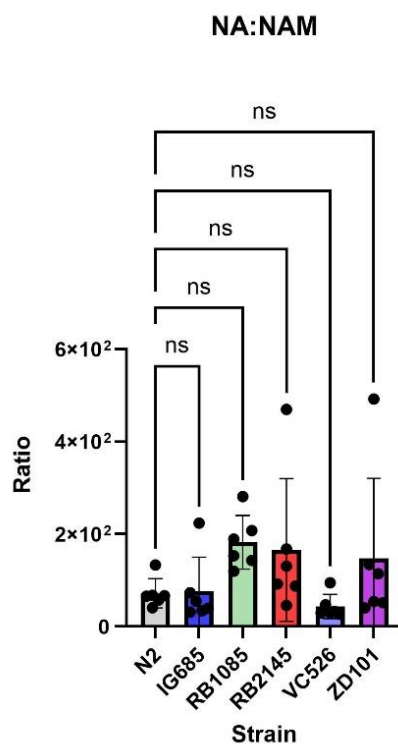


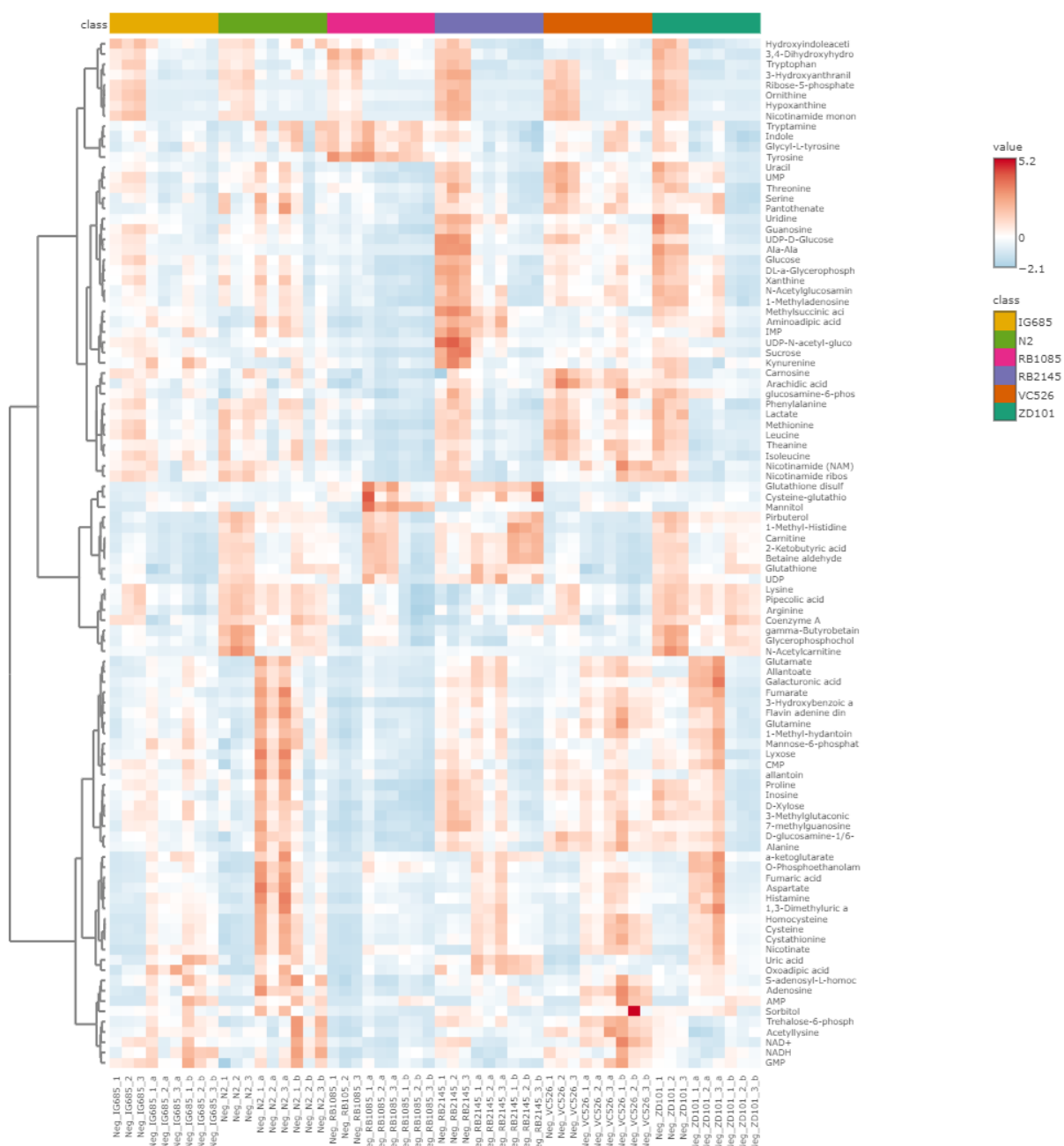
Figure 22: NAM to NA Turnover in TIR-1 Mutant Strains

Though not statistically significant, the ratio of NAM that converts to NA increases in strains RB1085, RB2145, and ZD101, one-way ANOVA

Role of TIR-1 in Global Metabolism

TIR-1 directly impacts NAD^+ metabolism and NAD^+ impacts global metabolism. To visualize how TIR-1 mutations regulate the entire metabolome, I created Figure 23 of heatmaps that display the relative values of every metabolite for which I obtained a good LC-MS readout.

A. Heatmap of All Biological and Technical Replicates



B. Heatmap of Averaged Biological and Technical Replicates

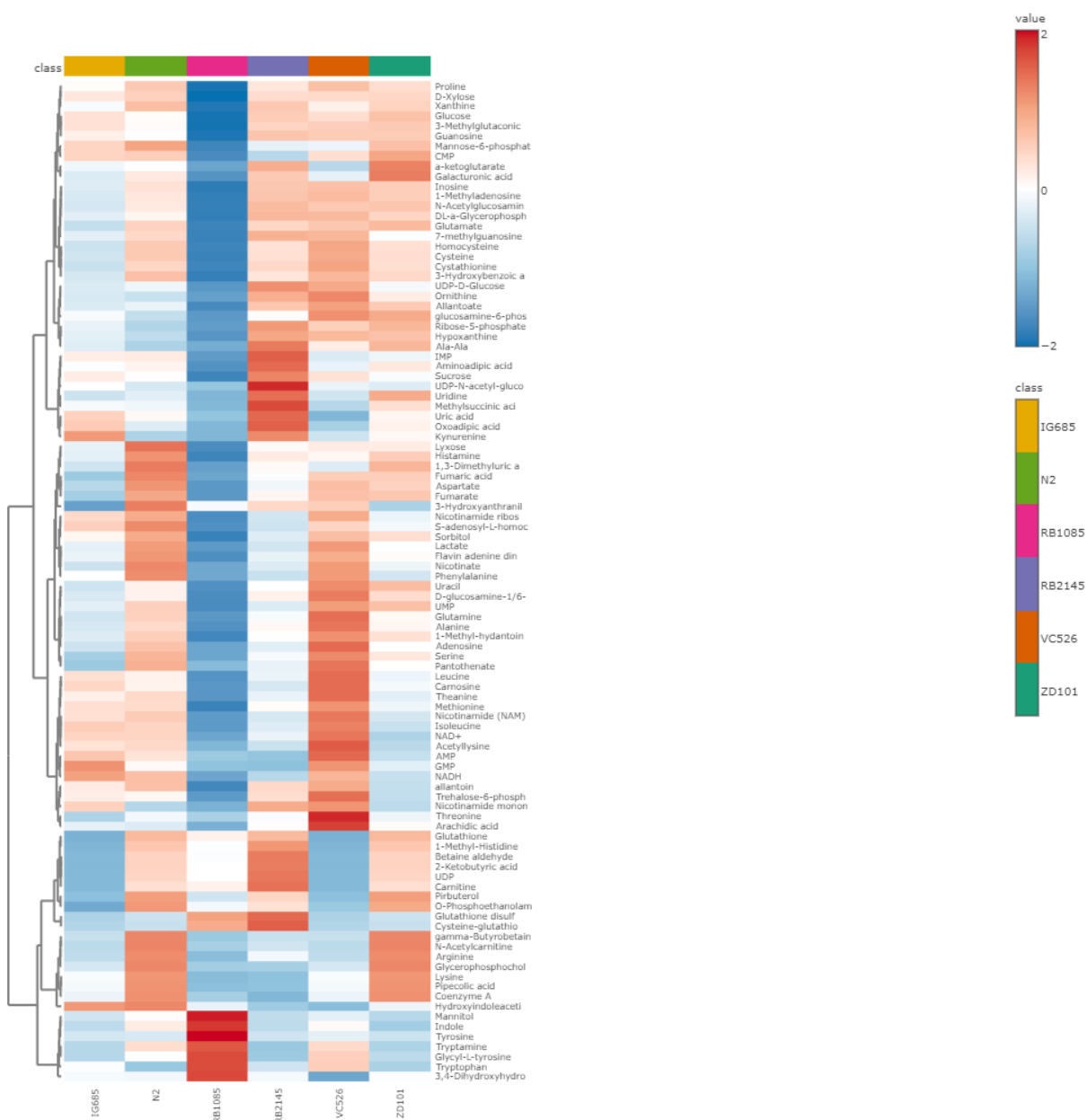


Figure 23: Global Metabolite Heatmaps

Chapter 4

Discussion

Necessity of Standardizing Longevity Assay Graphs

When comparing the average longevity of my strains, I chose to present my data in two forms: a comparison of biological replicate averages, and a comparison of the total average once I pooled replicated data together. Driven by the statistical power of a high number of cheap and expendable worms, the latter comparison yielded four significant p-values from formerly non-significant data. No obvious consensus exists on how researchers should collect or present *C. elegans* longevity data, yet the distinctions determine statistical validity.

I counted a biological replicate as an assay performed anew, beginning after the conclusion of the previous assay. When I scored my strains for brood-size and longevity, I maintained 20-30 animals per strain, each on their own plate. I defined each plate as a technical replicate.

Another researcher may define a biological replicate as a group of worms on one plate and each worm a technical replicate. With two plates of 10-15 worms each, that researcher could collect double the number of biological replicates while studying the same total number of worms.

My method is inefficient; after studying a total of seventy worms per strain, the numbers average into only three values to plot on a graph. The other researcher's method could double his statistical significance at the expense of validity. With even minor changes in temperature and

environment impacting *C. elegans* behavior, it may be misleading to collect multiple biological replicates at the same time. There must be a consensus compromise between valid data collection and efficient data collection to compare results between papers more accurately.

The lifespan data I collected indicates that TIR-1 mutations affect average longevity and lifespan more than the current literature suggests. When I pooled my longevity data, mutant strains VC526, ZD101, and RB2145 lived shorter lives on average than the wild-type strain. RB1085 lived longer. Because I did not repeat my experiments for the RB2145 and RB1085 strains, the data may not be accurate. Still, when most of the TIR-1 mutant strains live shorter lives, the data cautions against knockdown therapeutics.

Compared to average longevity measurements, Kaplan-Meier survival curves better represent an organism's lifespan and healthspan—the time an organism is healthy, not just alive. Kaplan-Meier curves, for example, would detect the difference between a population of one group that dies in infancy and another that dies in old age versus a population that dies in middle age. The two populations share an average lifespan, but there is more nuance; after infancy, the former population is healthier than the latter. By depicting the probability of survival through a given period rather than the average time of death, Kaplan-Meier curves offer a means to statistically compare frequency distributions of time of death.

The Mantel-Cox test of the Kaplan-Meier curves statistically confirmed a difference in the lifespans (not necessarily the longevities) of the TIR-1 mutant strains. The test statistic

corresponds to the difference in the Gaussian distribution curves for each strain, though the Gaussian curves would fit the data more neatly with a greater sample size.

Despite the awkward trend-line, the frequency graphs reveal a role for TIR-1 that the longevity graphs could not. In the N2 strain, not a single worm died before day nine, but over half the sample died by day fourteen. *C. elegans* lay 80% of their brood by day eight⁴⁸, meaning that all N2 worms survived to lay their full brood. The least healthy died shortly thereafter while the healthiest made it past day twenty.

In the mutant strains, worms died prior to day nine, indicating that the stress of childbirth killed the least healthy worms before they lay a full brood. Meanwhile, the healthiest mutant worms reached the same old age as the healthiest N2 worms. Because TIR-1 mutants died disproportionately during childbirth, there is support for the hypothesis that TIR-1 plays a protective role during periods of stress.

Reproductive Assays as Measurements of Stress-Tolerance

The brood-size assay may not represent reproductive health so much as it indicates stress tolerance. If the TIR-1 mutation disrupts worm metabolism, worms may conserve resources by allocating less energy into childbirth. In other words, the reproductive health assay requires assays that measure energy expenditure to understand if reproductive health is worse or if energy expenditure overall is worse.

Movement assays under a tracker and swimming assays could provide metrics for how much energy the worms choose to expend versus how much energy the worms *can* expend. These assays could also help contextualize the metabolic data. If the mutant worms conserve energy by moving less and having fewer children, then their metabolic readouts may look more similar to the N2 strain than they otherwise would have been.

Interestingly, while brood size decreased across all TIR-1 mutant strains, it decreased the least in the IG685 strain. The IG685 strain contains a full TIR-1 deletion. A partially functional TIR-1 may be more adverse than a dysfunctional TIR-1—a pattern that extends to internal hatching.

Internal hatching, another readout for reproductive health, demonstrated a sharp increase in the TIR-1 mutants. N2 worms rarely internally hatch, though stressful conditions including bacterial infection or starvation induce the phenotype, perhaps because the parent's body provides enough food for the progeny to reach to a resistant dauer stage⁴⁹.

Because internal hatching correlates with stress and reduced longevity even in individuals that do not internally hatch, its frequency reliably reports population-wide stress⁴⁹. The increase in internal hatching in the TIR-1 mutant strains may further indicate the lower stress tolerance in TIR-1 mutants. Another possibility for the increase is that without TIR-1, the mutants are more susceptible to bacterial infection. Performing brood-assays on UV-killed food may help answer if increased bacterial infection causes the increased internal hatching.

Statistical Significance of Metabolomic Data

I performed three biological replicates of the multigenerational life-food metabolomics experiment. Each biological replicate contained technical replicates of three unique samples from a strain. Although I collected the samples and extracted the metabolites on different weeks for each biological replicate, I ran biological replicates two and three at the same time in the LC-MS machine. The LC-MS detected higher metabolite levels in first three technical replicates, corresponding to biological replicate number one, compared to the final six technical replicates, corresponding to the final two biological replicates that I analyzed together.

I first tried normalizing the data from each of the first three technical replicates against the N2 strain, but the total counts still did not match the normalized values for the final six technical replicates. Because statistical analysis requires at least three data points, I decided to analyze the six technical replicates from trials two and three, excluding the outliers.

Because each of the technical replicates comes from a unique population of multigenerational worms, variation comes from biological differences rather than machine variation. The difference in the samples I omitted, however, comes from the machine performing differently on different days, not necessarily from biological variation. Therefore, I believe that my data gains validity by omitting the first biological replicate and comparing the remaining six technical replicates.

TIR-1 Shunts Tryptophan into the *De Novo* Pathway

My analysis of NAD⁺ metabolism begins before reaching an NAD⁺ pathway. Tryptophan can commit to three directions: the indole pathway, the serotonin pathway, or the kynurenine pathway (also known as the *de novo* pathway). The LC-MS data suggests that TIR-1 modulates which pathway tryptophan chooses. The percentage of tryptophan that commits to the kynurenine pathway increases for strains IG685, RB2145, and ZD101. In those same strains, the percentage of tryptophan that commits to the indole pathway does not change. Though I did not obtain readouts from the serotonin pathway, tryptophan must shunt away from the serotonin pathway into the kynurenine pathway in the TIR-1 mutants.

TIR-1 Shunts Kynurenine out of the *De Novo* Pathway

The 3-hydroxyanthranilic acid:kynurenine ratio proved that in all of the mutants except for RB1085, a smaller percent of kynurenine converted into 3-hydroxyanthranilic acid compared to the wild-type strain. There are two possibilities for why that happens: either kynurenine shunts out of the *de novo* pathway by forming other metabolites, or one of the enzymes that processes kynurenine to 3-hydroxyanthranilic acid downregulates.

In the latter hypothesis, kynurenine increases like the level of water in a running sink when the drain is clogged—creation without consumption. If the increase in kynurenine exactly correlated to the decrease in 3-hydroxyanthranilic acid, then I could show that instead of shunting out of the *de novo* pathway, kynurenine levels simply pool in the sink basin. By normalizing levels of kynurenine in the mutants by the levels in N2, I calculated the relative increase of pooled

kynurenine in the sink basin. By normalizing 3-hydroxyanthranilic acid to levels in N2, I calculated the relative decrease of water running out of the drain.

Because the relative increase in kynurenine did not correlate to the relative decrease in 3-hydroxyanthranilic acid, I disprove the clogged drain hypothesis. Or at least, if kynurenine does pool in the sink, it soon finds somewhere else to go. Better readouts of the metabolites branching off the kynurenine pathway would be useful in determining which pathways kynurenine (or the kynurenine and 3-hydroxyanthranilic acid intermediary, 3-hydroxykynurenine) shunts into and why.

Immune Pathways and *De Novo* Regulation

Of the five enzymes in the kynurenine pathway that convert tryptophan into quinolinic acid, three are regulated by cytokines⁵⁰. Cytokines also regulate several of the enzymes that shunt *de novo* metabolites out of the *de novo*⁵⁰. Cytokines like interleukins, interferons, and TNF alpha signal infection, promoting the inflammation response in immune cells. Because TIR-1 mediates the innate immune system, altered cytokine expression in the TIR-1 mutants may control the differential regulation of the *de novo* path. Future metabolomic experiments conducted on worms grown on UV killed food could prevent infection from altering the pathway.

Oxidation in TIR-1 Mutants

In three of the mutants, IG685, RB2145, and ZD101, 3-hydroxyanthranilic acid levels plummeted. Studies in *C. elegans* demonstrate that 3-hydroxyanthranilic acid resists oxidative stress and that animals supplemented with the metabolite live longer⁵¹. In addition to a decline in the 3-hydroxyanthranilic acid antioxidant, TIR-1 mutant worms display higher NAD⁺/NADH and glutathione disulfide:glutathione ratios. These ratios are shifted towards the oxidized species, indicating that TIR-1 may provide a protective role by reducing oxidative stress.

Altered NR Pathway in TIR-1 Mutants

I discovered a decline in NMN and NAD⁺ in the TIR-1 mutants that corresponded proportionally to a decline in NR. It seems unlikely that the enzyme that converts NR to NMN upregulates, since neither the levels of NMN, NAD⁺, nor any of the metabolites in the salvage pathway increase.

Recent studies in humans suggest that another enzyme, purine nucleoside phosphorylase (NP), converts NR into NAM. If the NAM:NAD⁺ ratio increased in the TIR-1 mutants, I could hypothesize that an undiscovered *C. elegans* NP homologue upregulates in the absence of TIR-1. However, the NAM:NAD⁺ ratio remains even across the strains. Because NAM levels change proportionally to NAD⁺, then NR cannot also be breaking down into NAM.

Without evidence of increased NR consumption, I hypothesize that TIR-1 regulates NR uptake from the diet. Supplementing the N2 and TIR-1 mutant strains with NR could reveal if the

mutants struggle to accept the metabolite. In a clinical context, NR supplementation could alleviate metabolic stress caused by therapeutics which knockdown SARM1.

A Lackluster NAD⁺ Consumer

NR levels, not reduced NAD⁺ consumption, seem to determine the amount NAD⁺ in the TIR-1 mutant strains. Although NAM—the direct breakdown product of NAD⁺—decreases in some of the TIR-1 mutant strains, the unchanging NAM: NAD⁺ ratio proves that NAM levels decline because NAD⁺ levels declined, not because of reduced consumer activity.

AMP and ribose 5-phosphate indirectly correspond to NAD⁺ consumption. Their levels should increase when TIR-1 breaks NAD⁺ into ADPR, but metabolites other than ADPR form AMP and ribose 5-phosphate as well. Further, their readouts may indicate SARM1 activity better than TIR-1 activity because 90% of SARM1's break down product becomes ADPR, while 90% of TIR-1's break down product spontaneously cyclizes into cADPR—a metabolite that does not turn into AMP or ribose 5-phosphate. Still, following my reasoning for determining the NAM: NAD⁺ ratio, I determined the AMP: NAD⁺ ratio and ribose 5-phosphate:NAD⁺ ratio, finding that they did not decline either.

Because my data does not show any significant decline in NAD⁺ breakdown products when normalized for NAD⁺ levels, it seems that TIR-1 is not a major NAD⁺ consumer in the worm. This data also refutes the hypothesis that TIR-1 covers the roles of SARM1 and CD38 in the worm, because in humans, CD38 is the most prolific NAD⁺ consumer⁵². Future research could

explore these readouts for strains put under stress including age, infection, or neuron injury to see if TIR-1 becomes a bigger player in NAD^+ consumption. Because TIR-1 is constitutively active while SARM1 reacts to the $\text{NMN}:\text{NAD}^+$ ratio, I expect that stress would upregulate SARM1 activity more than it would upregulate TIR-1 activity.

Overactive Salvage Pathway

Although NAM turnover did not statistically deviate from the wild-type strain, the recycling rate trends higher in strains RB1085, RB2145, and ZD101. Two of those strains, RB2145 and ZD101, displayed low levels of the *de novo* metabolite, 3-hydroxyanthranilic acid because kynurenine shunted away from the *de novo* pathway. When the salvage and *de novo* pathways converge at NaMN, they seem to even each other out: while RB1085, RB2145, and ZD101 trend slightly lower than N2, the difference is not statistically significant. With more replicates, the trending data may gain the statistical power to show that the salvage pathway upregulates to compensate for a downregulated *de novo* pathway.

Appendix

List of Abbreviations in Order of Appearance

- NAD⁺ - Nicotinamide Adenine Dinucleotide
- NADH - Nicotinamide Adenine Dinucleotide + Hydrogen
- PARPs – Poly ADP-Ribosyl Polymerases
- CD38 – Cyclic ADP-Ribose Synthase 38
- SARM1 – Sterile Alpha and TIR Motif Containing 1
- TIR Domain - Toll/Interleukin-1 Receptor Domain
- *C. elegans* - *Caenorhabditis elegans*
- MAPK – Mitogen-Activated Protein Kinase
- Ca²⁺ - Calcium Ion
- NaMN – Nicotinic Acid Mononucleotide
- NA – Nicotinic Acid
- NAM – Nicotinamide
- NMN – Nicotinamide Mononucleotide
- NR – Nicotinamide Riboside
- NMNAT1 – Nicotinamide Nucleotide Adenylyltransferase 1
- NMNAT 2 - Nicotinamide Nucleotide Adenylyltransferase 2
- JNK – c-Jun N-terminal Kinase
- ATP – Adenosine Triphosphate
- ARM Domain – Armadillo Repeat Domain

- SAM Domain – Sterile Alpha Motif Domain
- ADPR – Adenosine Diphosphate Ribose
- cADPR – Cyclic Adenosine Diphosphate Ribose
- Cryo-EM – Cryogenic Electron Microscopy
- NGM Agar – Nematode Growth Medium Agar
- *E. coli* – *Escherichia Coli*
- L4 – Larval Stage 4
- LC-MS – Liquid Chromatography Coupled Mass Spectrometry
- HILIC – Hydrophilic Interaction Chromatography
- BCA Assay – Bicinchoninic Acid Assay
- 3-HAA - 3-Hydroxyanthranilic Acid
- AMP – Adenosine Monophosphate

Funding Acknowledgment

This work was supported by the following grants:

- Howard Hughes Medical Institute Hanna H. Gray Fellows Program Faculty Phase (Grant# GT15655)
- Burroughs Wellcome Fund PDEP Transition to Faculty (Grant# 1022604)

BIBLIOGRAPHY

- (1) Dattani, S.; Rodés-Guirao, L.; Ritchie, H.; Ortiz-Ospina, E.; Roser, M. Life Expectancy, 2023. <https://ourworldindata.org/life-expectancy>.
- (2) Roser, M. It's Not Just about Child Mortality, Life Expectancy Increased at All Ages. <https://ourworldindata.org/its-not-just-about-child-mortality-life-expectancy-improved-at-all-ages#article-citation>.
- (3) Fang, J.; Chen, W.; Hou, P.; Liu, Z.; Zuo, M.; Liu, S.; Feng, C.; Han, Y.; Li, P.; Shi, Y.; Shao, C. NAD⁺ Metabolism-Based Immunoregulation and Therapeutic Potential. *Cell Biosci.* **2023**, *13* (1), 81. <https://doi.org/10.1186/s13578-023-01031-5>.
- (4) Zhang, M.; Ying, W. NAD⁺ Deficiency Is a Common Central Pathological Factor of a Number of Diseases and Aging: Mechanisms and Therapeutic Implications. *Antioxid. Redox Signal.* **2019**, *30* (6), 890–905. <https://doi.org/10.1089/ars.2017.7445>.
- (5) Aman, Y.; Qiu, Y.; Tao, J.; Fang, E. F. Therapeutic Potential of Boosting NAD⁺ in Aging and Age-Related Diseases. *Transl. Med. Aging* **2018**, *2*, 30–37. <https://doi.org/10.1016/j.tma.2018.08.003>.
- (6) McReynolds, M. R.; Chellappa, K.; Chiles, E.; Jankowski, C.; Shen, Y.; Chen, L.; Descamps, H. C.; Mukherjee, S.; Bhat, Y. R.; Lingala, S. R.; Chu, Q.; Botolin, P.; Hayat, F.; Doke, T.; Susztak, K.; Thaiss, C. A.; Lu, W.; Migaud, M. E.; Su, X.; Rabinowitz, J. D.; Baur, J. A. NAD⁺ Flux Is Maintained in Aged Mice despite Lower Tissue Concentrations. *Cell Syst.* **2021**, *12* (12), 1160-1172.e4. <https://doi.org/10.1016/j.cels.2021.09.001>.
- (7) Zhao, L.; Cao, J.; Hu, K.; He, X.; Yun, D.; Tong, T.; Han, L. Sirtuins and Their Biological Relevance in Aging and Age-Related Diseases. *Aging Dis.* **2020**, *11* (4), 927. <https://doi.org/10.14336/AD.2019.0820>.

- (8) Guo, S.; Zhang, S.; Zhuang, Y.; Xie, F.; Wang, R.; Kong, X.; Zhang, Q.; Feng, Y.; Gao, H.; Kong, X.; Liu, T. Muscle PARP1 Inhibition Extends Lifespan through AMPK α PARylation and Activation in *Drosophila*. *Proc. Natl. Acad. Sci.* **2023**, *120* (13), e2213857120. <https://doi.org/10.1073/pnas.2213857120>.
- (9) Peclat, T. R.; Thompson, K. L.; Warner, G. M.; Chini, C. C. S.; Tarragó, M. G.; Mazdeh, D. Z.; Zhang, C.; Zavala-Solorio, J.; Kolumam, G.; Liang Wong, Y.; Cohen, R. L.; Chini, E. N. CD38 Inhibitor 78c Increases Mice Lifespan and Healthspan in a Model of Chronological Aging. *Aging Cell* **2022**, *21* (4), e13589. <https://doi.org/10.1111/ace1.13589>.
- (10) Grabowska, W.; Sikora, E.; Bielak-Zmijewska, A. Sirtuins, a Promising Target in Slowing down the Ageing Process. *Biogerontology* **2017**, *18* (4), 447–476. <https://doi.org/10.1007/s10522-017-9685-9>.
- (11) Waller, T. J.; Collins, C. A. Multifaceted Roles of SARM1 in Axon Degeneration and Signaling. *Front. Cell. Neurosci.* **2022**, *16*, 958900. <https://doi.org/10.3389/fncel.2022.958900>.
- (12) Bradshaw, D. V.; Knutsen, A. K.; Korotcov, A.; Sullivan, G. M.; Radomski, K. L.; Dardzinski, B. J.; Zi, X.; McDaniel, D. P.; Armstrong, R. C. Genetic Inactivation of SARM1 Axon Degeneration Pathway Improves Outcome Trajectory after Experimental Traumatic Brain Injury Based on Pathological, Radiological, and Functional Measures. *Acta Neuropathol. Commun.* **2021**, *9* (1), 89. <https://doi.org/10.1186/s40478-021-01193-8>.
- (13) Tian, W.; Czopka, T.; López-Schier, H. Systemic Loss of Sarm1 Protects Schwann Cells from Chemotoxicity by Delaying Axon Degeneration. *Commun. Biol.* **2020**, *3* (1), 49. <https://doi.org/10.1038/s42003-020-0776-9>.
- (14) Cheng, Y.; Liu, J.; Luan, Y.; Liu, Z.; Lai, H.; Zhong, W.; Yang, Y.; Yu, H.; Feng, N.; Wang, H.; Huang, R.; He, Z.; Yan, M.; Zhang, F.; Sun, Y.-G.; Ying, H.; Guo, F.; Zhai, Q. *Sarm1* Gene Deficiency Attenuates Diabetic Peripheral Neuropathy in Mice. *Diabetes* **2019**, *68* (11), 2120–2130. <https://doi.org/10.2337/db18-1233>.

- (15) Miao, X.; Wu, Q.; Du, S.; Xiang, L.; Zhou, S.; Zhu, J.; Chen, Z.; Wang, H.; Pan, X.; Fan, Y.; Zhang, L.; Qian, J.; Xing, Y.; Xie, Y.; Hu, L.; Xu, H.; Wang, W.; Wang, Y.; Huang, Z. SARM1 Promotes Neurodegeneration and Memory Impairment in Mouse Models of Alzheimer's Disease. *Aging Dis.* **2024**, *15* (1), 390–407. <https://doi.org/10.14336/AD.2023.0516-1>.
- (16) Essuman, K.; Summers, D. W.; Sasaki, Y.; Mao, X.; DiAntonio, A.; Milbrandt, J. The SARM1 Toll/Interleukin-1 Receptor Domain Possesses Intrinsic NAD⁺ Cleavage Activity That Promotes Pathological Axonal Degeneration. *Neuron* **2017**, *93* (6), 1334-1343.e5. <https://doi.org/10.1016/j.neuron.2017.02.022>.
- (17) Irazoqui, J. E.; Urbach, J. M.; Ausubel, F. M. Evolution of Host Innate Defence: Insights from *Caenorhabditis Elegans* and Primitive Invertebrates. *Nat. Rev. Immunol.* **2010**, *10* (1), 47–58. <https://doi.org/10.1038/nri2689>.
- (18) Belinda, L. W.-C.; Wei, W. X.; Hanh, B. T. H.; Lei, L. X.; Bow, H.; Ling, D. J. SARM: A Novel Toll-like Receptor Adaptor, Is Functionally Conserved from Arthropod to Human. *Mol. Immunol.* **2008**, *45* (6), 1732–1742. <https://doi.org/10.1016/j.molimm.2007.09.030>.
- (19) DiAntonio, A.; Milbrandt, J.; Figley, M. D. The SARM1 TIR NADase: Mechanistic Similarities to Bacterial Phage Defense and Toxin-Antitoxin Systems. *Front. Immunol.* **2021**, *12*, 752898. <https://doi.org/10.3389/fimmu.2021.752898>.
- (20) Nimma, S.; Gu, W.; Maruta, N.; Li, Y.; Pan, M.; Saikot, F. K.; Lim, B. Y. J.; McGuinness, H. Y.; Zaoti, Z. F.; Li, S.; Desa, S.; Manik, M. K.; Nanson, J. D.; Kobe, B. Structural Evolution of TIR-Domain Signalosomes. *Front. Immunol.* **2021**, *12*, 784484. <https://doi.org/10.3389/fimmu.2021.784484>.
- (21) O'Neill, L. A. J.; Bowie, A. G. The Family of Five: TIR-Domain-Containing Adaptors in Toll-like Receptor Signalling. *Nat. Rev. Immunol.* **2007**, *7* (5), 353–364. <https://doi.org/10.1038/nri2079>.
- (22) Lee, E.; Redzic, J. S.; Nemkov, T.; Saviola, A. J.; Dzieciatkowska, M.; Hansen, K. C.; D'Alessandro, A.; Dinarello, C.; Eisenmesser, E. Z. Human and Bacterial Toll-Interleukin Receptor

Domains Exhibit Distinct Dynamic Features and Functions. *Molecules* **2022**, *27* (14), 4494.

<https://doi.org/10.3390/molecules27144494>.

(23) Peterson, N. D.; Icsó, J. D.; Salisbury, J. E.; Rodríguez, T.; Thompson, P. R.; Pukkila-Worley, R. Pathogen Infection and Cholesterol Deficiency Activate the C. Elegans P38 Immune Pathway through a TIR-1/SARM1 Phase Transition. *eLife* **2022**, *11*, e74206. <https://doi.org/10.7554/eLife.74206>.

(24) Bradshaw, P. Cytoplasmic and Mitochondrial NADPH-Coupled Redox Systems in the Regulation of Aging. *Nutrients* **2019**, *11* (3), 504. <https://doi.org/10.3390/nu11030504>.

(25) Glaría, E.; Valledor, A. F. Roles of CD38 in the Immune Response to Infection. *Cells* **2020**, *9* (1), 228. <https://doi.org/10.3390/cells9010228>.

(26) Lee, H. C.; Zhao, Y. J. Resolving the Topological Enigma in Ca²⁺ Signaling by Cyclic ADP-Ribose and NAADP. *J. Biol. Chem.* **2019**, *294* (52), 19831–19843.

<https://doi.org/10.1074/jbc.REV119.009635>.

(27) Schmitt, F.; Eckert, G. P. Caenorhabditis Elegans as a Model for the Effects of Phytochemicals on Mitochondria and Aging. *Biomolecules* **2022**, *12* (11), 1550.

<https://doi.org/10.3390/biom12111550>.

(28) Emmons, S. W.; Yemini, E.; Zimmer, M. Methods for Analyzing Neuronal Structure and Activity in Caenorhabditis Elegans. *Genetics* **2021**, *218* (4), iyab072.

<https://doi.org/10.1093/genetics/iyab072>.

(29) Kimble, J.; Nüsslein-Volhard, C. The Great Small Organisms of Developmental Genetics: Caenorhabditis Elegans and Drosophila Melanogaster. *Dev. Biol.* **2022**, *485*, 93–122.

<https://doi.org/10.1016/j.ydbio.2022.02.013>.

(30) Lee, Y.; Jeong, H.; Park, K. H.; Kim, K. W. Effects of NAD⁺ in Caenorhabditis Elegans Models of Neuronal Damage. *Biomolecules* **2020**, *10* (7), 993. <https://doi.org/10.3390/biom10070993>.

- (31) Loring, H. S.; Thompson, P. R. Emergence of SARM1 as a Potential Therapeutic Target for Wallerian-Type Diseases. *Cell Chem. Biol.* **2020**, *27* (1), 1–13.
<https://doi.org/10.1016/j.chembiol.2019.11.002>.
- (32) Osterloh, J. M.; Yang, J.; Rooney, T. M.; Fox, A. N.; Adalbert, R.; Powell, E. H.; Sheehan, A. E.; Avery, M. A.; Hackett, R.; Logan, M. A.; MacDonald, J. M.; Ziegenfuss, J. S.; Milde, S.; Hou, Y.-J.; Nathan, C.; Ding, A.; Brown, R. H.; Conforti, L.; Coleman, M.; Tessier-Lavigne, M.; Züchner, S.; Freeman, M. R. dSarm/Sarm1 Is Required for Activation of an Injury-Induced Axon Death Pathway. *Science* **2012**, *337* (6093), 481–484. <https://doi.org/10.1126/science.1223899>.
- (33) Murata, H.; Khine, C. C.; Nishikawa, A.; Yamamoto, K.-I.; Kinoshita, R.; Sakaguchi, M. C-Jun N-Terminal Kinase (JNK)-Mediated Phosphorylation of SARM1 Regulates NAD⁺ Cleavage Activity to Inhibit Mitochondrial Respiration. *J. Biol. Chem.* **2018**, *293* (49), 18933–18943.
<https://doi.org/10.1074/jbc.RA118.004578>.
- (34) Kim, Y.; Zhou, P.; Qian, L.; Chuang, J.-Z.; Lee, J.; Li, C.; Iadecola, C.; Nathan, C.; Ding, A. MyD88-5 Links Mitochondria, Microtubules, and JNK3 in Neurons and Regulates Neuronal Survival. *J. Exp. Med.* **2007**, *204* (9), 2063–2074. <https://doi.org/10.1084/jem.20070868>.
- (35) Czech, V. L.; O'Connor, L. C.; Philippon, B.; Norman, E.; Byrne, A. B. TIR-1/SARM1 Inhibits Axon Regeneration and Promotes Axon Degeneration. *eLife* **2023**, *12*, e80856.
<https://doi.org/10.7554/eLife.80856>.
- (36) Figley, M. D.; Gu, W.; Nanson, J. D.; Shi, Y.; Sasaki, Y.; Cunnea, K.; Malde, A. K.; Jia, X.; Luo, Z.; Saikot, F. K.; Mosaiab, T.; Masic, V.; Holt, S.; Hartley-Tassell, L.; McGuinness, H. Y.; Manik, M. K.; Bosanac, T.; Landsberg, M. J.; Kerry, P. S.; Mobli, M.; Hughes, R. O.; Milbrandt, J.; Kobe, B.; DiAntonio, A.; Ve, T. SARM1 Is a Metabolic Sensor Activated by an Increased NMN/NAD⁺ Ratio to Trigger Axon Degeneration. *Neuron* **2021**, *109* (7), 1118–1136.e11.
<https://doi.org/10.1016/j.neuron.2021.02.009>.

- (37) Yang, J.; Wu, Z.; Renier, N.; Simon, D. J.; Uryu, K.; Park, D. S.; Greer, P. A.; Tournier, C.; Davis, R. J.; Tessier-Lavigne, M. Pathological Axonal Death through a MAPK Cascade That Triggers a Local Energy Deficit. *Cell* **2015**, *160* (1–2), 161–176. <https://doi.org/10.1016/j.cell.2014.11.053>.
- (38) Li, Y.; Pazyra-Murphy, M. F.; Avizonis, D.; de Sá Tavares Russo, M.; Tang, S.; Chen, C.-Y.; Hsueh, Y.-P.; Bergholz, J. S.; Jiang, T.; Zhao, J. J.; Zhu, J.; Ko, K. W.; Milbrandt, J.; DiAntonio, A.; Segal, R. A. Sarm1 Activation Produces cADPR to Increase Intra-Axonal Ca⁺⁺ and Promote Axon Degeneration in PIPN. *J. Cell Biol.* **2022**, *221* (2), e202106080. <https://doi.org/10.1083/jcb.202106080>.
- (39) Sporny, M.; Guez-Haddad, J.; Khazma, T.; Yaron, A.; Dessau, M.; Shkolnisky, Y.; Mim, C.; Isupov, M. N.; Zalk, R.; Hons, M.; Opatowsky, Y. Structural Basis for SARM1 Inhibition and Activation under Energetic Stress. *eLife* **2020**, *9*, e62021. <https://doi.org/10.7554/eLife.62021>.
- (40) Khazma, T.; Golan-Vaishenker, Y.; Guez-Haddad, J.; Grossman, A.; Sain, R.; Weitman, M.; Plotnikov, A.; Zalk, R.; Yaron, A.; Hons, M.; Opatowsky, Y. A Duplex Structure of SARM1 Octamers Stabilized by a New Inhibitor. *Cell. Mol. Life Sci.* **2023**, *80* (1), 16. <https://doi.org/10.1007/s00018-022-04641-3>.
- (41) McReynolds, M. R.; Chellappa, K.; Baur, J. A. Age-Related NAD⁺ Decline. *Exp. Gerontol.* **2020**, *134*, 110888. <https://doi.org/10.1016/j.exger.2020.110888>.
- (42) Miranda-Vizueté, A.; Veal, E. A. *Caenorhabditis Elegans* as a Model for Understanding ROS Function in Physiology and Disease. *Redox Biol.* **2017**, *11*, 708–714. <https://doi.org/10.1016/j.redox.2016.12.020>.
- (43) Hayakawa, T.; Kato, K.; Hayakawa, R.; Hisamoto, N.; Matsumoto, K.; Takeda, K.; Ichijo, H. Regulation of Anoxic Death in *Caenorhabditis Elegans* by Mammalian Apoptosis Signal-Regulating Kinase (ASK) Family Proteins. *Genetics* **2011**, *187* (3), 785–792. <https://doi.org/10.1534/genetics.110.124883>.
- (44) Liberati, N. T.; Fitzgerald, K. A.; Kim, D. H.; Feinbaum, R.; Golenbock, D. T.; Ausubel, F. M. Requirement for a Conserved Toll/Interleukin-1 Resistance Domain Protein in the *Caenorhabditis*

Elegans Immune Response. *Proc. Natl. Acad. Sci.* **2004**, *101* (17), 6593–6598.

<https://doi.org/10.1073/pnas.0308625101>.

(45) Khazma, T.; Grossman, A.; Guez-Haddad, J.; Feng, C.; Dabas, H.; Sain, R.; Weitman, M.; Zalk, R.; Isupov, M. N.; Hammarlund, M.; Hons, M.; Opatowsky, Y. Structure-Function Analysis of ceTIR-1/hSARM1 Explains the Lack of Wallerian Axonal Degeneration in *C. Elegans*. *Cell Rep.* **2023**, *42* (9), 113026. <https://doi.org/10.1016/j.celrep.2023.113026>.

(46) Wu, Z.; Isik, M.; Moroz, N.; Steinbaugh, M. J.; Zhang, P.; Blackwell, T. K. Dietary Restriction Extends Lifespan through Metabolic Regulation of Innate Immunity. *Cell Metab.* **2019**, *29* (5), 1192-1205.e8. <https://doi.org/10.1016/j.cmet.2019.02.013>.

(47) Darlington, L. G.; Forrest, C. M.; Mackay, G. M.; Smith, R. A.; Smith, A. J.; Stoy, N.; Stone, T. W. On the Biological Importance of the 3-Hydroxyanthranilic Acid: Anthranilic Acid Ratio. *Int. J. Tryptophan Res. IJTR* **2010**, *3*, 51–59. <https://doi.org/10.4137/ijtr.s4282>.

(48) Muschiol, D.; Schroeder, F.; Traunspurger, W. Life Cycle and Population Growth Rate of *Caenorhabditis Elegans* Studied by a New Method. *BMC Ecol.* **2009**, *9* (1), 14. <https://doi.org/10.1186/1472-6785-9-14>.

(49) Mosser, T.; Matic, I.; Leroy, M. Bacterium-Induced Internal Egg Hatching Frequency Is Predictive of Life Span in *Caenorhabditis Elegans* Populations. *Appl. Environ. Microbiol.* **2011**, *77* (22), 8189–8192. <https://doi.org/10.1128/AEM.06357-11>.

(50) Mithaiwala, M. N.; Santana-Coelho, D.; Porter, G. A.; O'Connor, J. C. Neuroinflammation and the Kynurenine Pathway in CNS Disease: Molecular Mechanisms and Therapeutic Implications. *Cells* **2021**, *10* (6), 1548. <https://doi.org/10.3390/cells10061548>.

(51) Dang, H.; Castro-Portuguez, R.; Espejo, L.; Backer, G.; Freitas, S.; Spence, E.; Meyers, J.; Shuck, K.; Gardea, E. A.; Chang, L. M.; Balsa, J.; Thorns, N.; Corban, C.; Liu, T.; Bean, S.; Sheehan, S.; Korstanje, R.; Sutphin, G. L. On the Benefits of the Tryptophan Metabolite 3-Hydroxyanthranilic

Acid in *Caenorhabditis Elegans* and Mouse Aging. *Nat. Commun.* **2023**, *14* (1), 8338.

<https://doi.org/10.1038/s41467-023-43527-1>.

(52) Chini, C. C. S.; Peclat, T. R.; Warner, G. M.; Kashyap, S.; Espindola-Netto, J. M.; De Oliveira, G. C.; Gomez, L. S.; Hogan, K. A.; Tarragó, M. G.; Puranik, A. S.; Agorrody, G.; Thompson, K. L.; Dang, K.; Clarke, S.; Childs, B. G.; Kanamori, K. S.; Witte, M. A.; Vidal, P.; Kirkland, A. L.; De Cecco, M.; Chellappa, K.; McReynolds, M. R.; Jankowski, C.; Tchkonina, T.; Kirkland, J. L.; Sedivy, J. M.; Van Deursen, J. M.; Baker, D. J.; Van Schooten, W.; Rabinowitz, J. D.; Baur, J. A.; Chini, E. N. CD38 Ecto-Enzyme in Immune Cells Is Induced during Aging and Regulates NAD⁺ and NMN Levels. *Nat. Metab.* **2020**, *2* (11), 1284–1304. <https://doi.org/10.1038/s42255-020-00298-z>.